

*Dear Editor,*

*on behalf of the co-authors, I would like to thank you for having handled the review and the open discussion of our manuscript.*

*We acknowledge also the Executive Editor and the two anonymous referees for their constructive comments and suggestions, which allowed us to improve our work.*

*Below, the point by point replies to the comments of the referees and the list of all relevant changes made to the manuscript. Please note that the indication of pages and lines of the text refer to the version of the manuscript published in GMDD.*

*Furthermore, attached you'll find the last version (revised) of the manuscript with tables and figures. In this version all the changes added made to the manuscript are highlighted in red.*

*As requested by the Executive Editor, a new section named "Code Availability" was added at the end of the manuscript.*

*Sincerely,*

*Stefano Luigi Gariano*

## Replies to Anonymous Referee #1

*Authors are grateful to the Referee #1 for his/her precious suggestions and comments. Below, please find the changes to the text and replies for each issue raised.*

Some issues should be better focused, with a more extended discussion:

1) runoff for unsaturated soils (pag. 1227, line 23), a discussion could be useful with reference to the suction-runoff dependence highlighted by Cuomo and Della Sala (2013, Eng. Geol. Journal) and similar contributions.

*Following referee's suggestion, we propose to modify the text as specified below.*

At page 1227, line 20, after “evapo-transpiration and runoff processes”, insert: “The combination of rainfall infiltration and runoff may cause different types of mass-movements (either slope failure or erosion processes) depending on the intensity and duration of the rainfall and the values of soil suction (Cuomo and Della Sala, 2013)”.

At page 1231, line 12: at the end of the sentence “..looks less important.” please add “In addition, as underlined by Cuomo and Della Sala (2013), among other authors, in unsaturated shallow deposits, time to runoff, time to failure and runoff rates strongly depend on soil water characteristic curves, soil initial conditions, rainfall intensity and slope angle. Moreover, soil mechanical parameters affect the time to failure that can result either shorter or longer than time to runoff.”

2) definition of "medium-scale" landslides is not provided. Do you mean medium-size landslide or what? Please refer to any landslide classification for basic definitions.

*Actually, we meant a medium-size landslide (all the occurrences in the text have been accordingly modified).*

*In addition, by following Hutchinson's proposal (1995), the “deep-seatedness” of the case study could be classified as “intermediate” (being the estimated maximum vertical depth of the surface of rupture from the ground surface,  $V_{max}$ , equal to ca. 25 m).*

At page 1244, lines 15-18: please change “The rock slide shows a medium-scale size (maximum width = 200 m, length > 650 m), and involves Late Miocene conglomerate..” into “The rock slide is of medium-size (maximum width = 200 m, length > 650 m, estimated maximum vertical depth = 25 m), with a deep-seatedness factor (*sensu* Hutchinson, 1995) that may be classified as “intermediate”. It involves Late Miocene conglomerate..”

Page 1226, line 15: replace “medium-scale” with “medium-size”.

Page 1228 line 22: replace “medium-scale” with “medium-size”.

Page 1245, line 20: replace “medium-depth” with “medium-size”.

Page 1245, line 26: replace “medium-scale” with “medium-size”.

Page 1249, line 5: replace “medium-scale” with “medium-size”.

Page 1250, line 13: replace “medium-depth” with “medium-size”.

3) a special characteristic of shallow soil covers in Campania region is not much evidenced: that is the unsaturated conditions of soils, whose suction is seasonally variable. For this issue, you can summarise the main results of Cascini et al. (2014, Landslides) about the seasonal effects of rainfall and soil suction for slope stability

At page 1241, after line 23, please insert the following sentence:

Rainfall-induced shallow landslides are widespread in the pyroclastic soils covering the slopes of the study area. Among the various factors affecting the spatial distribution and the type of slope instability, Cascini et al. (2014) pointed out that both the rainfall conditions and the consequent seasonal variations of soil suction play a significant role. In particular, when suction is low and frontal rainfall occurs (from November to May) first time shallow landslides are triggered; when suction is high or very high and convective or hurricane-type rainfall occurs (from June to October) mostly erosion phenomena occur, often turning into hyperconcentrated flows.

At page 1242, line 25, please insert the following sentence

Shallow landslides listed in Table 1 occurred between November and March, a period characterised by a medium to low suction range and included in the rainy season (October to April) according to Cascini et al. (2014). The same Authors pointed out that, in this period, frontal rainfall typically occurs and may trigger widespread first-time shallow landslides later propagating as debris flow or debris avalanches.

#### *References:*

*Cascini, L., Sorbino, G., Cuomo, S., Ferlisi, S.: Seasonal effects of rainfall on the shallow pyroclastic deposits of the Campania region (southern Italy), Landslides, 11, 779–792, 2014.*

*Cuomo, S. and Della Sala, M.: Rainfall-induced infiltration, runoff and failure in steep unsaturated shallow soil deposits, Eng. Geol., 162, 118-127, 2013.*

*Hutchinson, J.N.: Deep-seated mass movements on slopes, Mem. Soc. Geol. It., 50, 147-164, 1995.*

## Replies to Anonymous Referee #2

*Authors are grateful to the Referee #2 for his/her comments and interesting suggestions. Below, please find our replies to each issue raised, and the proposed changes to the text.*

1) First, the adopted fitness definition deserves a more robust discussion and motivation in the manuscript. Moreover, the authors should mention if they performed an investigation on alternative metrics. In fact, according to the literature, the adopted fitness can significantly affect the results of calibration procedures, both in terms of achieved maximum and potential overfitting (which affects validation accuracy).

*We agree with the Referee, and propose to extend the discussion on the adopted fitness, also providing an example of computation, by including the following sentences.*

Page 1240, after line 4:

“For instance, if two dates of activation are available, the obtained fitness is  $\Phi_u = 1 + \frac{1}{2} = 1.5$  if both are well captured by the mobility function (i.e. they correspond to the highest peaks). On the other hand, in case only one of the dates is captured and the remaining one ranks fifth,  $\Phi_u = 1 + \frac{1}{5} = 1.2$ .”

Page 1252, after line 10:

“In this study, a 2-steps efficiency criterion was employed: the relative position of the peaks of the mobility function with respect to the dates of landslide activation was first considered, and the fitness computed. Based on the value of  $\Delta Z_{cr}$ , the obtained solutions were further ranked. Average, synthetic filter functions can then be computed by selecting the best 100 kernels for successive validation purposes. Alternative metrics (cf., among the others, Krause et al., 2005) for the fitness function are being tested. However, due to uncertainties concerning input data (i.e. rainfall and dates of landslide activation), the adoption of sophisticated techniques does not sound very promising. In addition, problems of over-fitting may depend on both data uncertainties and number of parameters. Commonly, kernels characterized by a complex pattern (and then by many parameters) are needed for simulating groundwater dynamics (Pinault et al., 2001). Nevertheless, more complex kernels do not necessarily imply higher predictive uncertainties (Fienen et al., 2010; Long, 2015). Still, the adopted discrete approach allows focusing only on the timing of the peaks of the mobility function, thus somehow relieving the computational effort. Due to the cited uncertainties in input data, a “temporal window” was in fact employed to help matching dates of activation with the peaks of the mobility function. Further attempts of defining the fitness function by different metrics, and the analysis of its effects on calibration and validation, are being considered against another case study (San Benedetto Ullano, in Calabria, Southern Italy), whose mobility phases have been recently monitored by the same authors (Iovine et al., 2010; Capparelli et al., 2012).”

2) As for the family of “optimal kernels”, my advice is to better explain such a concept.

In fact, a single-objective GA typically provides a single optimal (or “best”) individual, thus the mentioned concept of “family of optimal kernels” provided by the procedure can confuse the reader.

The same applies to the concept of “average kernels” introduced in section 5. Currently, the reader has to struggle to understand why the authors average kernels when they have a “best kernel”, or what is the origin of the 100 averaged kernels.

*We agree with the Referee, but up to date - in the performed experiments related to real case studies - we never got a single “best solution” much better than the rest. Commonly, a set of optimal solutions with rather similar fitness were instead obtained. That is why we chose to average a number of individuals to synthesize the kernel to be used for validation. Accordingly, we propose to extend the discussion both on the family of optimal kernels and on the average kernel, by including the following period.*

Page 1241, after line 6:

“Differently from what usually experienced in rainfall-runoff models, <sup>GA</sup>SAKE therefore provide multiple

equivalent solutions - i.e. a number of optimal kernels with same fitness,  $\Phi_u$ , despite different shapes. This may depend on the limited number of available dates of activations, and on other noises in input data (e.g. rain gauges located too far from the site of landslide activation; inaccurate information on dates of activation or on the phenomenon). The adoption of synthetic kernels – e.g. obtained by averaging a suitable set of optimal kernels – allows to synthesize the family of results for successive practical applications: in this work, the best 100 kernels obtained for each case study were in fact utilized to synthesize average kernels to be employed for validation purposes.”

3) Also, in section 6, it is not clear why the progressive calibration procedure was also labelled as “self-adaptive”.

*The term “self-adaptive” was actually used to stress the ability of the model to react to input changes, such as new dates of landslide activations and more prolonged rainfall series. This feature represents a major advantage of the model. In particular, the self-adaptive procedure of progressive calibration was performed by considering an increasing number of dates of activation to mimic the adoption of the model in a landslide warning system. Obtained results underlined how <sup>GA</sup>SAKe easily self-adapt to external changes by optimizing its performances with increasing fitness values. To better explain the above issues, we would propose to modify the manuscript as follows.*

Page 1248, line 5, replace “simulate the occurrence of known landslide activations” with “to react and self-adapt to input changes, like new dates of landslide activation.”

Page 1248, line 7, replace “In particular,” with “To simulate the adoption of <sup>GA</sup>SAKe in a landslide warning system.”

Page 1251, line 5, at the end of the sentence, please add: “Accordingly, the results of the progressive procedure underlined how <sup>GA</sup>SAKe can easily self-adapt to external changes by optimizing its performances, providing increasing fitness values”.

#### *References:*

*Capparelli, G., Iaquina, P., Iovine, G., Terranova, O.G., and Versace P.: Modelling the rainfall-induced mobilization of a large slope movement in northern Calabria, Nat. Hazards, 61(1), 247–256, 2012.*

*Fienen, M.N., Doherty, J.E., Hunt, R.J., and Reeves, H.W.: Using prediction uncertainty analysis to design hydrologic monitoring networks: example applications from the Great Lakes water availability pilot project, US Geol. Surv., Reston Virginia, Scientific Investigations Report 2010–5159, 44 pp., 2010.*

*Iovine, G., Lollino, P., Gariano, S.L., and Terranova, O.G.: Coupling limit equilibrium analyses and real-time monitoring to refine a landslide surveillance system in Calabria (southern Italy), Nat. Hazards Earth Syst. Sci., 10, 2341–2354, 2010.*

*Krause, P., Boyle D.P., and Båse, F.: Comparison of different efficiency criteria for hydrological model assessment, Adv Geosciences, 5, 89–97, 2005*

*Long, A.J.: RRAWFLOW: Rainfall-Response Aquifer and Watershed Flow Model (v1.15), Geosci. Model Dev., 8, 865–880, 2015.*

*Pinault, J.-L., Plagnes, V., and Aquilina, L.: Inverse modeling of the hydrological and the hydrochemical behavior of hydrosystems: Characterization of karst system functioning, Water Resour Res, 37(8), 2191–2204, 2001.*

## ***GA*SAKe : forecasting landslide activations by a Genetic-Algorithms based hydrological model**

*Oreste G. Terranova<sup>1</sup>, Stefano Luigi Gariano<sup>2,3\*</sup>, Pasquale Iaquineta<sup>1</sup> & Giulio G.R. Iovine<sup>1</sup>*

- <sup>1)</sup> CNR-IRPI (National Research Council – Research Institute for Geo-Hydrological Protection), via Cavour 6, 87036, Rende, Cosenza, Italia.
- <sup>2)</sup> CNR-IRPI (National Research Council – Research Institute for Geo-Hydrological Protection), via Madonna Alta 126, 06128, Perugia, Italia.
- <sup>3)</sup> University of Perugia, Department of Physics and Geology, via A. Pascoli, 06123, Perugia, Italia.

\*Corresponding Author: [gariano@irpi.cnr.it](mailto:gariano@irpi.cnr.it), Phone: +39 075 5014424.

### **ABSTRACT**

*GA*SAKe is a new hydrological model aimed at forecasting the triggering of landslides. The model is based on Genetic-Algorithms and allows to obtaining thresholds of landslide activation from the set of historical occurrences and from the rainfall series.

*GA*SAKe can be applied to either single landslides or set of similar slope movements in a homogeneous environment. Calibration of the model is based on Genetic Algorithms, and provides for families of optimal, discretized solutions (kernels) that maximize the fitness function. Starting from these latter, the corresponding mobility functions (i.e. the predictive tools) can be obtained through convolution with the rain series. The base time of the kernel is related to the magnitude of the considered slope movement, as well as to hydro-geological complexity of the site. Generally, smaller values are expected for shallow slope instabilities with respect to large-scale phenomena. Once validated, the model can be applied to estimate the timing of future landslide activations in the same study area, by employing recorded or forecasted rainfall series.

Example of application of *GA*SAKe to a **medium-size** slope movement (the Uncino landslide at San Fili, in Calabria, Southern Italy) and to a set of shallow landslides (in the Sorrento Peninsula, Campania, Southern Italy) are discussed. In both cases, a successful calibration of the model has been achieved, despite unavoidable uncertainties concerning the dates of landslide occurrence. In particular, for the Sorrento Peninsula case, a fitness of 0.81 has been obtained by calibrating the model against 10 dates of landslide activation; in the Uncino case, a fitness of 1 (i.e. neither missing nor false alarms) has been achieved against 5 activations. As for temporal validation, the experiments performed by considering the extra dates of landslide activation have also proved satisfactory.

In view of early-warning applications for civil protection purposes, the capability of the model to simulate the occurrences of the Uncino landslide has been tested by means of a progressive, self-adaptive procedure. Finally, a sensitivity analysis has been performed by taking into account the main parameters of the model.

The obtained results are quite promising, given the high performance of the model obtained against different types of slope instabilities, characterized by several historical activations. Nevertheless, further refinements are still needed for applications to landslide risk mitigation within early-warning and decision-support systems.

**Key words:** hydrological model, rainfall threshold, landslide triggering, genetic algorithm

## 1 INTRODUCTION

A nationwide investigation, carried out by the National Geological Survey, identified approximately  $5 \times 10^5$  slope movements in Italy, an average of 1.6 failures per square kilometre (Trigila, 2007).

According to other investigations, this figure would rather be a lower estimate (cf. Servizio Geologico, Sismico dei Suoli, 1999; Guzzetti et al., 2008). In the period 1950–2009, at least 6349 persons were killed, went missing, or were injured by landslides, with an average of 16 harmful events per year, thus confirming the notable risk posed to population (Guzzetti, 2000; Salvati et al., 2010).

Petley (2008) estimated that about 90% of worldwide casualties can be attributed to landslides triggered by rainfall. With reference to the Italian territory, about 70% of landslides result to be triggered by rainfall (cf. CNR-GNDCI **AVI** Project, Alfieri et al., 2012).

In more general terms, slope instability conditions are influenced by rainfall that, allowing infiltration into the slopes, cause temporary changes in groundwater dynamics (Van Asch et al., 1999). Actually, rainfall infiltrates the slopes only partially, the remaining aliquots being involved into evapo-transpiration and runoff processes. **The combination of rainfall infiltration and runoff may cause different types of mass-movements (either slope failure or erosion processes) depending on the intensity and duration of the rainfall and the values of soil suction (Cuomo and Della Sala, 2013).** Concentration of water deriving from either contemporary or antecedent storms at specific sites plays a major role in triggering landslides – as testified by slope instabilities that commonly follow the heaviest phases of rainfall events.

To model the relationships between rainfall and landslide occurrence, two distinct approaches are generally adopted in literature. The first, “complete” or “physically-based”, attempt to determine the influence of rainfall on slope stability by modelling its effects in terms of overland flow, groundwater infiltration, pore pressures and related balance of shear stress and resistance (cf. e.g. Montgomery and Dietrich, 1994; Wilson and Wieczorek, 1995; Crosta, 1998; Terlien, 1998; Crosta et al., 2003; Pisani et al., 2010). At this latter purpose, numerical models are employed, and a notable (and expensive) amount of detailed data is commonly required to define the geological scheme of the slope in litho-structural, hydrogeological, morphologic and geotechnical terms. The second approach (adopted in the present study), named “empirical” or “hydrological” (Cascini and Versace, 1988), is based on a statistical-probabilistic analysis of rainfall series and of dates of occurrence of landslide activation (see, among the others, Campbell, 1975; Caine, 1980; UNDRO, 1991; Sirangelo and Versace, 1996; Guzzetti et al., 2007; 2008, Brunetti et al. 2010, Gariano et al., 2015). Methodological examples in literature generally focus on thresholds obtained for *i*) single phenomena or *ii*) given types of slope movements within a homogeneous geo-environmental setting (cf. e.g. Jakob and Weatherly, 2003).

In this study, the hydrological model  $^{GA}SAKe$  (i.e., the Genetic-Algorithm based release of the model *Self Adaptive Kernel*) to forecast the triggering of slope movements is described. The model can be applied to either single landslides or to a set of similar phenomena within a homogeneous study area. Model calibration is performed by means of Genetic Algorithms: in this way, a family of optimal, discretized kernels can iteratively be obtained from initial tentative solutions. In another release of the model ( $^{CM}SAKe$  – i.e., *Cluster model SAKe*) the calibration could instead be performed through an iterative procedure (Terranova et al., 2013).

Examples of application of the model to a **medium-size** landslide (the Uncino landslide at San Fili) and to shallow slope movements in the Sorrento Peninsula are discussed in the following sections. Temporal validation is discussed for both cases, in view of early-warning applications of  $^{GA}SAKe$

for Civil Protection purposes. Moreover, a progressive, self-adaptive procedure of calibration and validation is discussed, by considering the Uncino case study, to verify changes in fitness, predictive ability and base time when an increasing number of dates of activation is employed. In addition, the results of preliminary, parametric analyses are presented, aimed at investigating the role of the main parameters of the model.

## 2 BACKGROUND

Physical systems evolve in time due to their own inner dynamics and/or as a consequence of external causes. Suitable observational tools can be employed to monitor their evolution. They can be arranged to promptly send reports or warnings to the authorities of civil protection to support the management of emergencies (Cauvin et al., 1998; for applications to landslides, cf. also Keefer et al., 1987; Iovine et al., 2009; Capparelli and Versace, 2011; Pradhan and Buchroithner, 2012). In the case of complex systems (e.g. nuclear power stations, telecommunication networks, etc.), many parameters, in part interdependent, have to be monitored. Missing an automated phase of analysis and proper filtering, a great number of reports may be delivered by the monitoring apparatus in few seconds. At this purpose, the concepts of threshold (Carter, 2010), event and warning must therefore be suitably defined.

Regarding slope movements, the notions of threshold and warning have long been investigated. In particular, a threshold constitutes a condition - generally expressed in quantitative terms or through a mathematical law - whose occurrence implies a change of state (White et al., 1996). According to the ALARM study group (Cauvin et al., 1998), an event is *i*) a portion of information extracted from either continuous or discrete signals (i.e. a significant variation), transmitted by a component of the monitoring network; or *ii*) a set of data concerning the considered context (e.g. restorations, actions, observations). According to such definition, an event must be instantaneous and dated. As for warning, its definition derives from that of event: it is a discrete indicator aimed at triggering a human or an automated reaction. The warning can be classified into distinct levels (e.g. in terms of security) or by type (e.g. related to a distinct component of the dynamic system under consideration), to be transmitted by the monitoring system.

In complex systems, causal factors responsible for emergency conditions may be difficult to identify. Therefore, warnings may be issued according to pre-fixed thresholds related to suitable physical properties of the system. In these cases, the timing of data sampling of the monitoring instruments should be progressively adapted to the evolution of the phenomenon. A further issue concerns the chances of missing alarms and of false alarms, as well as the camouflage of an alarm among simultaneous others.

In physical terms, slope instability can occur when the shear strength gets lower than a given threshold (Terzaghi, 1962). Rain infiltration may temporarily change the dynamics of ground water (Van Asch et al., 1999): due to an increase in pore water pressure, the effective shear strength of the material decreases, and a slope movement can be triggered.

Groundwater may reach a given location within the slope by different paths. The main natural mechanisms include: *i*) surface flow, strongly influenced by morphology; *ii*) direct infiltration from the surface; *iii*) flow within the soil mantle (*throughflow*) from upslope and sideslopes; *iv*) seepage from the bedrock toward the overlying colluvium. The length of the different paths may be quite different, and characterized by distinct velocities: as a consequence, aliquots of the same rainfall event may reach a given site at different times, variously combining with other groundwater amounts (Ellen, 1988).



Aiming at applying a hydrological approach, empirical relations have to be determined by means of thresholds to distinguish among conditions which likely correspond to landslide occurrence or not. To this aim, different hydrological parameters can be selected (Guzzetti et al., 2007; 2008 and <http://rainfallthresholds.irpi.cnr.it/>): the cumulative rain recorded in a given temporal window (hours/days/months) before landslide activation; the average rain intensity in the same temporal window; normalized rains to reference values (e.g. annual averages). Simplified hydrological balances can also be adopted in empirical approaches, by considering losses of aliquots of rains by run-off, evapo-transpiration, etc.

As concerns superficial landslide, triggering thresholds can be derived from relations between the “triggering” rain (daily, hourly or shorter), corresponding to the onset of the slope movement, and the cumulative rain in an antecedent period (usually, few days to two weeks before landslide activation) (e.g. Campbell, 1975; Cannon and Ellen, 1985; Wieczorek, 1987; Terlien, 1996; Crosta, 1998; Zêzere and Rodrigues, 2002). In other cases, thresholds refer to relations between rain intensity,  $I$ , and duration,  $D$ , (e.g., Brunetti et al., 2010, Berti et al., 2012, Peres and Cancelliere, 2014). In some studies, antecedent rains were also considered, allowing to obtain better results (e.g. Campbell, 1975). Larger amounts of antecedent rain should allow slope movements to be activated by less severe triggering storms. In general, a direct relationship between antecedent rain and landslide dimension can be observed (Cascini and Versace, 1986); though, in some peculiar conditions (e.g. Hong Kong case studies, caused by suction reduction - Brand et al., 1984) this is not the case, and the role of antecedent rains looks less important. **In addition, as underlined by Cuomo and Della Sala (2013), among other authors, in unsaturated shallow deposits, time to runoff, time to failure and runoff rates strongly depend on soil water characteristic curves, soil initial conditions, rainfall intensity and slope angle. Moreover, soil mechanical parameters affect the time to failure that can result either shorter or longer than time to runoff.**

Difficulties in hydrological modelling of landslides generally increase, due to physical and economic issues, when dealing with deeper and larger phenomena (Cascini and Versace, 1986). In such cases, landslide activation depends on the dynamics of deeper groundwater bodies. By the way, it is not by chance that most studies do refer to small and superficial slope movements. Large slope movements usually show complex relationships with rains, as different groundwater aliquots may combine and reach the site of landslide triggering. Depending on type (cf. dimension, material, kinematics, etc.), different hydrological mechanisms should be considered, thus limiting the possibility of generalization of the thresholds (Dikau and Schrott, 1999; Corominas, 2001; Marques et al., 2008). Again, the mobilization of deeper phenomena commonly requires greater rainfall amounts with respect to shallow landslides, spanned over longer periods (Aleotti, 2004; Terranova et al., 2004; Guzzetti et al., 2007; 2008;). In these cases, rain durations responsible for landslide activations commonly range from ca. 30 days to several months, even beyond a single rainy season (Brunsden, 1984; Van Asch et al., 1999; Gullà et al., 2004; Trigo et al., 2005).

To analyse the triggering conditions of slope movements – either shallow or deep-seated – a modelling approach can be employed that is based on the threshold concept. For landslides (e.g. Aleotti, 2004; Wieczorek and Glade, 2005; Terranova et al., 2004; Vennari et al., 2014), empirical thresholds can be expressed in terms of curves, delimiting the portion of the Cartesian plane which contains “all and only” the hydrological conditions related to known activations (cf. e.g. the  $I$ - $D$  chart proposed by Caine, 1980). A further improvement to this approach can be obtained by considering hydrological conditions not related to landslide activations (Crozier, 1997; Sengupta et al., 2010; Gariano et al., 2015).

In general, no changes of state are assumed to occur below the threshold ( $z_t$ ), while they do happen above it. Alternatively (Crozier, 1997), a range of conditions can be defined, delimited by:

- ✓ a lower threshold ( $z_{low}$ ), below which changes of state do never occur, and
- ✓ an upper threshold ( $z_{upp}$ ), above which changes always happen.

For values between  $z_{upp}$  and  $z_{low}$ , a probability of state change can be defined, essentially depending on *i*) the incompleteness of knowledge on the physical process under investigation, and *ii*) the incapacity of the model to fully replicate the behaviour of the same process. In probabilistic terms:

$$\begin{aligned} P(E_t) &= 0 \text{ for } z(t) < z_{low} \\ P(E_t) &= 1 \text{ for } z(t) > z_{upp} \\ P(E_t) &= G[z(t)] \text{ for } z_{low} \leq z(t) \leq z_{upp} \end{aligned} \quad (1)$$

in which:  $P$  is the probability of occurrence (1=success, 0=unsuccess);  $E_t$  is a process (succession of events) whose states change with time  $t$ ;  $z(t)$  is the value assumed, at time  $t$ , by the variable that determines the change of state;  $z_{low}$  and  $z_{upp}$  are the minimum and maximum thresholds, respectively;  $G[z(t)]$  is a probability function, monotonically increasing with  $t$  in the range ]0,1[.

In hydrological models, to express the influence of rainfalls on runoff and groundwater dynamics, a “kernel” (also named “filter function”) can be employed, usually defined in terms of simple, continuous analytical functions (Chow et al., 1988). In such a way, suitable weights can be assigned to the precipitations occurred in the last hours/days before a given geo-hydrological process (e.g. discharge, measured at a generic river cross section; landslide activation), as well as to earlier rains recorded weeks/months before. The following types of kernels are among the most utilized: Beta, Gamma, Nash, negative exponential distribution. Furthermore, in this type of models, the “base time” ( $t_b$ ) expresses a sort of memory with respect to rainfalls. For instance, in classic rainfall-runoff modelling,  $t_b$  defines the time of concentration, while in slope stability analyses it represents the time interval, measured backward from landslide activation, during which rainfall is deemed to effectively affect groundwater dynamics, contributing to destabilization.

To modelling slope stability, both the shape and the base time of the kernel must be properly selected by considering type and dimension of the investigated phenomena, as well as geo-structural and hydrogeological characteristics. Unfortunately, in several real cases, the above-mentioned analytical functions may fail in capturing the complexity of groundwater dynamics properly, as well as the related landslide activations. In this respect, the adoption of discretized kernels, automatically calibrated through iterative computational techniques, may offer effective solutions.

### 3 THE MODEL *GASAKe*

*GASAKe* is an empirical-hydrological model for predicting the activation of slope movements of different types. It is based on a classic threshold scheme: the exceedance of the threshold determines a change of state, i.e. the triggering of the landslide. The scheme is inspired from the *FLaIR* model (*F*orecasting *L*andslides *I*nduced by *R*ainfall), proposed by Sirangelo and Versace (1996): through changes of state in time, the variable  $z(t)$  assumes the meaning of “*mobilization function*”. In other terms, the values of  $z(t)$  depend on the amount of rain stored in the aquifer.

In hydrology, rainfall-runoff modelling is commonly performed by adopting a linear, steady scheme (Chow et al., 1988). Such approach implies that the transformation of rainfall in runoff can be described by an integral of convolution between a unitary impulsive response of the basin – the kernel,  $h(t)$  – and the rainfall,  $p(t)$ .

The *kernel* (*filter function*) represents the unitary volume influx in an infinitesimal period, and is defined as:

$$\int_0^{\infty} h(t)dt = 1 \quad (2)$$

in which  $h(t)=h(-t)$ ,  $h(t) \geq 0$ ,  $\forall t$ .

In practical applications, the lower bound ( $t=0$ ) corresponds to the beginning of the flood-wave rising, and the kernel assumes a finite duration ( $t_b$ ). The integral of convolution is therefore expressed as:

$$z(t) = \int_0^{t_b} h(t - \tau) p(\tau)d\tau = \int_0^{t_b} h(\tau) p(t - \tau)d\tau \quad (3)$$

in which  $z(t)$  represents the discharge at the time  $t$ . For a specific case study, the kernel can be determined by means of calibration procedures, by relating discharge measurements to rains.

In discretized terms, the elements of the kernel are characterized by width  $\Delta t$  and height  $h_i$ , and equation (3) can be written as:

$$z_u = \sum_{i=1}^u h_i \cdot p_{u-i+1} \cdot \Delta t \quad (4)$$

Sirangelo and Versace (1996) proved that the same approach may turn out promising also for slope-stability modelling. Capparelli and Versace (2011) stressed that the *I-D* chart of Caine (1980) corresponds to a kernel defined by a power function  $h(t) = a t^b$ , with  $b < 0$ . The main difficulty in exporting the well-established knowledge of rainfall-runoff modelling, usually based on many measurements, to rainfall-landslide modelling lies in the scarcity of adequate information for proper calibration. In the latter case, only few dates of activation are in fact commonly available (often with unsatisfactory details on location and phenomena), and the values of  $z(t)$  are unknown. From a mathematical point of view, such a problem can be handled by assuming that the timing of the maxima of  $z(t)$  corresponds to the dates of landslide activation. When studying the triggering conditions of landslides, calibration can be therefore performed by maximizing the mobilization function in correspondence of the dates of activation.

Scarcity of information inevitably reflects on the resulting kernel, whose shape may turn out highly indeterminate: different functions, or different parameters of the same function, can in fact maximize  $z(t)$  in correspondence of the dates of mobilization. Model optimization – and its reliable utilization for early-warning purposes – can turn out an awkward issue.

In this work, an innovative modelling approach – based on discretized kernels, automatically calibrated through iterative computational techniques – is proposed, which may help in facing the above-cited difficulties. For modelling purposes, the rainfall series and a coherent set of dates of landslide occurrence – either related to a given slope movement, or to a set of landslides of the same type in a homogeneous geo-environmental zone – must be given as input to *G<sup>A</sup>SAKe*.

Unfortunately, when dealing with the timing of occurrence, historical notices may refer either to portions of the considered phenomena or to entire landslide bodies. Therefore, dates should be properly selected to consider only consistent cases. Moreover, dates of activation are usually known with only a broad approximation: with respect to the reports, the actual timing of occurrence may be located backward (documents may assign a later date) or forward (in case of later, more relevant movements). For modelling purposes, it is then useful to specify a temporal window, lasting from an initial ( $d_{t-from}$ ) to a final date ( $d_{t-to}$ ), containing the presumable date of occurrence.

Rainfall series are commonly reconstructed from data recorded at rain gauges located in a reasonable proximity of the study area. The temporal window of the hydrological analysis is

defined by the intersection of *i*) the period of observation of the rains and *ii*) that delimited by the ancientmost and the recentmost dates of activation of the landslide. A potential source of uncertainty lies in the fact that, occasionally, the considered rain gauge records amounts that notably differ from those actually experienced at landslide location. Furthermore, landslide triggering may also be due to causes different from rainfall (e.g. human activity, earthquakes): a thorough preliminary analysis must always be performed to verify the significance of rainfall preceding landslide activation, to detecting cases not to be considered in the hydrological study. In the model, rains older than  $t_b$  are neglected. Suitable maximum and minimum values ( $t_{b-max}$  and  $t_{b-min}$ ) must be initialized to allow the model to determine optimal values. Commonly,  $t_b$  ranging from few hours to some weeks are suggested for shallow landslides, while greater values (up to several months) sound suitable for deep-seated phenomena.

Based on the geological knowledge of the phenomenon under investigation, the initial shape of the kernel can be selected among a set of basic types. Among these, *i*) a “rectangular” shape can be adopted if older precipitations must have the same weight of more recent rains; *ii*) a “decreasing triangular”, if older precipitations are assumed to have a progressively smaller weight than more recent rains; *iii*) “increasing triangular”, if older precipitations are assumed to have a progressively greater weight than more recent rains. A casual shape or any other function can also be implemented in the model (e.g., Beta, Gamma, Nash, Negative exponential distribution).

### 3.1 Model Calibration

In  $GA_{SAKe}$ , model calibration is performed against real case studies through Genetic Algorithms (GAs). These latter are general-purpose, iterative search algorithms inspired by natural selection and genetics (Holland, 1975). Since 1970's, GAs have been applied to several fields of research, from applied mathematics (Poon and Sparks, 1992), to evolution of learning (Hinton and Nowlan, 1987), evolutionary robotics (Nolfi and Marocco, 2001), and debris-flow modelling (Iovine et al., 2005; D'Ambrosio et al., 2006). GAs simulate the evolution of a population of candidate solutions to a given problem by favouring the reproduction of the best individuals. The candidate solutions are codified by genotypes, typically using strings, whose elements are called genes.

GAs explore the solution space, defined as the set of all possible values of the genes. At the beginning of a given optimization experiment, the members of the initial population of genotypes (in this study, the *kernels*) are usually generated at random. The performance of each solution, in terms of phenotype (i.e. the *mobilization function*), is evaluated by applying a suitable *fitness function*, so determining its “adaptability”, i.e. the measure of its goodness in resolving the problem. The sequence of random genetic operators “selection, crossover and mutation”, constrained by prefixed probabilities, constitutes a single GA-iteration that generates a new population of candidate solutions. At each iteration, best individuals are in fact chosen by applying the selection operator. To form a new population of offspring, crossover is employed by combining parents' genes. Mutation is successively applied to each gene, by randomly changing its value within the allowed range.

Thanks to the GA approach, better individuals (i.e. characterized by higher fitness values) can be obtained over time. In fact, according to individual probabilities of selection, any change that increases the fitness tends to be preserved over the GA iterations (Holland, 1975). For further details on GAs, cf. Goldberg (1989) and Mitchell (1996).

In the present study, a steady-state and elitist GA (cf. De Jong, 1975) was employed to obtain the family of optimal kernels that maximize the mobility function in correspondence with known dates

of landslide activations. The procedure employed for calibration of  $GA\text{SAKe}$  is schematized in Figure 1.

At the beginning of an optimization experiment, the initial population of  $N$  kernels is generated at random, and the fitness of the related mobility functions is evaluated (cf. below). In order to evolve the initial population of candidate solutions and progressively obtaining better solutions, a total number of  $A$  GA-iterations follows.

At each iteration of the GA, the operators selection, crossover and mutation are applied as follows (Fig. 2):

- *selection*

- i.  $n_e$  “elitist” individuals are merely copied in a “mating pool” from the previous generation, by choosing the best ones;
- ii. the remaining  $N-n_e$  candidate solutions are chosen by applying the “*tournament without replacement*” selection operator. More in detail, a series of tournaments are performed by selecting two individuals at random from the previous generation: the winner (i.e. the one characterized by the highest fitness) is copied into the mating pool, according to a prefixed surviving probability ( $p_s$ ), which is set greater for the fittest individual. Note that, when choosing the  $N-n_e$  candidate solutions, a given individual cannot be selected more than once.

- *crossover*

After the mating pool is filled with  $N$  individuals, the crossover operator is applied, according to a prefixed probability ( $p_c$ ):

- i. two parent individuals are chosen from the mating pool at random;
- ii. a cutting point (*crossover point*) is then selected at random in the range  $]t_{b-min}, t_{b-max}[$ ;
- iii. the so-obtained portions of parents’ strings are exchanged, thus mixing the genetic information and resulting in two children (Fig. 3).

When the crossover is not applied, the two parents are merely copied into  $P_{new}$ .

- *mutation*

Based on a prefixed probability ( $p_m$ ), a random number of elements of the kernel ( $p_{me}$ , expressed as a percentage of  $t_b$ ) is mutated, by adding to each element an amount  $dh$  that is randomly obtained in the range  $[p_{mh1}, p_{mh2}]$ , as a function of the maximum value of the kernel ( $h_{max}$ ). Then  $dh$  ranges from  $dh_1$  to  $dh_2$ :

$$\begin{aligned} dh_1 &= p_{mh1} \cdot h_{max} \\ dh_2 &= p_{mh2} \cdot h_{max} \end{aligned} \tag{5}$$

Furthermore, the base time is also mutated (increased or decreased) within the bounds  $[t_{b-min}, t_{b-max}]$ , according to a random factor  $dt_b$  selected in the range  $[1/p_{mtb}, p_{mtb}]$  (Fig. 4).

Note that the children obtained after both crossover and mutation must be normalized, before they can be included in the population  $P_{new}$ , by properly scaling the elements of the kernels to ensure validity of equation 2.

During calibration, the shape of the kernel and its  $t_b$  are iteratively refined. Note that the shape is not subject to any constraint, while  $t_b$  is allowed to vary in the range  $[t_{b-min} - t_{b-max}]$ . The fitness is computed for each examined mobilization function, and new populations of kernels are generated as described above.

As for the fitness function, in  $GA\text{SAKe}$  it is defined as follows:

- the  $L$  available dates of landslide activation – as derived from the historical analyses – are arranged in a vector  $\mathcal{S} = \{S_1, S_2, \dots, S_i, \dots, S_L\}$ ;

- the vector of the relative maxima of the mobility function,  $\mathbf{Z} = \{z_1, z_2, \dots, z_j, \dots, z_M\}$ , is sorted in decreasing order ( $M$  = number of relative maxima);
- the vector of the partial fitness is  $\boldsymbol{\varphi} = \{\varphi_1, \varphi_2, \dots, \varphi_i, \dots, \varphi_L\}$ , where  $\varphi_i = k^{-l}$  depends on the rank  $k$  of the relative maxima of  $z_j$  that coincide with known dates of activation  $S_i$ . In case  $S_i$  does not correspond to any relative maximum, it is  $\varphi_i = 0$ .

With reference to a given kernel, the resulting fitness is expressed by  $\Phi_u = \sum_{i=1}^L \varphi_i$ . Aiming at generalizing the results for easier comparison to other study cases, a normalized fitness index is adopted,  $\Phi = \Phi_u / \Phi_{max}$ , defined in the range  $[0,1]$ , being  $\Phi_{max} = \sum_{i=1}^L 1/i$ .

For instance, if two dates of activation are available, the obtained fitness is  $\Phi_u = 1 + 1/2 = 1.5$  if both are well captured by the mobility function (i.e. they correspond to the highest peaks). On the other hand, in case only one of the dates is captured and the remaining one ranks fifth,  $\Phi_u = 1 + 1/5 = 1.2$ . Thanks to the above procedure, a family of “optimal kernels” which maximizes the fitness can be determined. The mobility function is in fact forced toward a shape characterized by relative maxima ( $z_j$ ) coinciding with the dates of landslide occurrence ( $S_i$ ). An optimal solution leads to a mobility function having the highest peaks in correspondence with such dates; further peaks may also be present, characterized by lower values. Nevertheless, kernel solutions generally determine mobility functions whose highest peaks only partly match with the dates of landslide occurrence (i.e. some dates may not correspond to the highest peaks nor to any peak at all).

To selecting the most suitable kernel from a given family of optimal ones, let's define:

- $z_{j-min}$  as the lowest of the peaks of the mobility function in correspondence with one of the dates of activation ( $S_i$ );
- $z_{cr}$  as the “critical threshold”, i.e. the highest peak of the mobility function just below  $z_{j-min}$ ;
- the “safety margin”,  $\Delta z_{cr} = (z_{j-min} - z_{cr}) / z_{j-min}$ .

When applying the fitness function to evaluate a given kernel, either incompleteness or low accuracy of input data may lead to “false alarms” – i.e. peaks of the mobility function ( $z_j$ ) which are greater than the threshold  $z_{cr}$ , but do not correspond to any of the known dates of activation. Such alarms can actually be of two different types: 1) “untrue false”, due to an informative gap in the archive (i.e. correct prediction); 2) “true false”, in case of real misprediction of the model. On such cases, further historical investigations may help to discriminating between the mentioned types of false alarms.

Also depending on the specific purpose of the analysis, the most suitable kernel can therefore be selected by one or more of the following criteria: *i*) the greatest  $\Delta z_{cr}$ ; *ii*) the shortest  $t_b$ ; *iii*) the smallest  $\mu_0 = \sum_{i \leq t_b} (i - 0.5) h_i \Delta t$ , i.e. the first-order momentum of the kernel with respect to the vertical axis. The first criterion allows for activating early-warning procedures with greatest advance; the remaining ones (to be employed when  $\Delta z_{cr}$  is too small) generally correspond to more impulsive responses to rainfall.

Differently from what usually experienced in rainfall-runoff models, <sup>GA</sup>SAKe therefore provide multiple equivalent solutions - i.e. a number of optimal kernels with same fitness,  $\Phi_u$ , despite different shapes. This may depend on the limited number of available dates of activations, and on other noises in input data (e.g. rain gauges located too far from the site of landslide activation; inaccurate information on dates of activation or on the phenomenon). The adoption of synthetic kernels – e.g. obtained by averaging a suitable set of optimal kernels – allows to synthesize the family of results for successive practical applications: in this work, the best 100 kernels obtained for

each case study were in fact utilized to synthesize average kernels to be employed for validation purposes.

## 4 CASE STUDIES

The case studies considered in this paper are: *i*) a set of shallow landslides in the Sorrento Peninsula between Gragnano and Castellammare di Stabia (Campania, Southern Italy); and *ii*) the Uncino landslide at San Fili (Calabria, Southern Italy).

Note that, as the numbers of known historical activations in the study areas were adequate, some dates could be excluded from calibration, and were successively employed for validation purposes. In particular, the recentmost dates of landslide activation (cf. Tables 1 and 2) were considered to validate the “average kernels” (see below), as obtained from the families of optimal solutions defined through calibration. The procedure employed for validation is schematized in Figure 5.

### 4.1 Shallow landslides in the Sorrento Peninsula - Campania

The Sorrento Peninsula is located in western Campania, Southern Italy (Fig. 6). In the area, Mesozoic limestone mainly crop out, covered by Miocene flysch, Pleistocene volcanic deposits (pyroclastic fall, ignimbrite), and Pleistocene detritical-alluvial deposits (Di Crescenzo and Santo, 1999). The carbonate bedrock constitutes a monocline, gently dipping towards WNW, mantled by sedimentary and volcanoclastic deposits, with thickness ranging from few decimetres to tens of meters.

Rainfall-induced shallow landslides are widespread in the pyroclastic soils covering the slopes of the study area. Among the various factors affecting the spatial distribution and the type of slope instability, Cascini et al. (2014) pointed out that both the rainfall conditions and the consequent seasonal variations of soil suction play a significant role. In particular, when suction is low and frontal rainfall occurs (from November to May) first time shallow landslides are triggered; when suction is high or very high and convective or hurricane-type rainfall occurs (from June to October) mostly erosion phenomena occur, often turning into hyperconcentrated flows.

The study area is characterized by hot, dry summers and moderately cold and rainy winters. Consequently, its climate can be classified as Mediterranean (Csa in the Köppen-Geiger's classification). In particular, the mean annual temperature ranges from 8-9°C, at the highest elevations of M. Faito and M. Cerreto, to 17-18°C along coasts and valleys. Average annual rainfall varies from 900 mm west of Sorrento to 1500 mm at M. Faito; moving inland to the East, it reaches 1600 mm at M. Cerreto and 1700 mm at the Chiunzi pass (Ducci and Tranfaglia, 2005). On average, annual totals are concentrated in about 95 rainy days. During the driest six months (from April to September), only 30% of the annual rainfall is recorded in about 30 rainy days. During the three wettest months (November, October, and December), a similar amount is recorded in about 34 rainy days (Servizio Idrografico, 1948-1999). In the area, convective rainstorms may occur, characterized by a very high intensity, at the beginning of the rainy season (from September to October). In Autumn-Winter, either high intensity or long duration rainfall are usually recorded, while uniformly distributed rains generally occur in Spring (Fiorillo and Wilson, 2004). As for annual maxima of daily rainfall recorded at the sea level, the Amalfi coast (southern border of the Sorrento Peninsula) is characterized by smaller values (59 mm) of average annual maxima of daily rainfall than the Sorrento coast (86 mm), on the northern border. Such difference seems to persist even at higher elevations (up to 1000 m a.s.l.), with 84 mm vs. 116 mm for the southern and northern mountain slopes, respectively (Rossi and Villani, 1994).

Severe storms frequently affect the study area, triggering shallow landslides that propagate seaward, often causing casualties and serious damage to urbanized areas and transportation facilities (Mele and Del Prete, 1999; Calcaterra and Santo, 2004; Di Crescenzo and Santo, 2005). In the second half of the XX century, several shallow landslides activated nearby Castellammare di Stabia: in Table 1, the major events recorded between Vico Equense and Gragnano are listed, with details on types of events, affected sites and references. **Shallow landslides listed in Table 1 occurred between November and March, a period characterised by a medium to low suction range and included in the rainy season (October to April) according to Cascini et al. (2014). The same Authors pointed out that, in this period, frontal rainfall typically occurs and may trigger widespread first-time shallow landslides later propagating as debris flow or debris avalanches.**

Rainfall responsible for landslide occurrences in the Sorrento Peninsula are shown in Fig. 7, in terms of cumulated antecedent rains, extracted from the records of the nearest gauges (Tramonti, Castellammare, and Tramonti-Chiunzi – cf. Fig. 6). The trends of antecedent rains look quite differentiated, ranging from abrupt (cf. curves 5, 6, 7) to progressive increases (cf. 2, 4, 10). On the other hand, the curve 0 does not highlight significant amounts of rainfall in the 14 days preceding landslide activation: therefore, the occurrence recorded on 14 April 1967 was excluded by the hydrological analysis. Quite moderate amounts of cases 6 and 7 (occurred on 4 November 1980 and 14 November 1982, resp.) were instead recorded in short periods, thus resulting into high-intensity events that could be considered as triggering factor of the observed landslides.

As a result, the dates of activation from #1 to #10 were selected for calibration, whilst #11 was employed for validation. As shallow landslides were being considered, the rainfall period employed for calibration spanned from 17 January 1963 to 10 December 1996; for validation, the rainfall series terminates on 10 February 1997 – i.e. the validation date  $+t_b$  (this latter as obtained from calibration).

#### **4.2 The Uncino landslide - San Fili (Northern Calabria)**

San Fili (Fig. 8) is located on the western margin of the Crati *graben*, a tectonic depression belonging to the active Calabrian-Sicilian Rift Zone (Monaco and Tortorici, 2000). In the area, vicarious, N-S trending normal faults mark the base of the Coastal Chain, at the transition between Palaeozoic metamorphic rocks, to the west, and Pliocene-Quaternary sediments, to the east (Amodio Morelli et al., 1976). Nearby San Fili, Palaeozoic migmatitic gneiss and biotitic schist, generally weathered, are mantled by a Late Miocene sedimentary cover of reddish continental conglomerates, followed by marine sandstone and clays (CASMEZ, 1967).

In particular, the village lies in the intermediate sector between the two faults, marked by a NE-SW trending connection fault, delimiting the Miocene sediments on the north from the gneissic rocks on the South.

The Calabrian Tyrrhenian sector (including the study area) results rainier than the Ionian (about 1200-2000 mm vs. 500 mm), although the most severe storms are more frequently recorded on the Ionian sector (Terranova, 2004). The average annual temperature is about 15°C: the coldest months are January and February (in average 5°C), followed by December (8°C); the hottest months are July and August (24°C), followed by June (22°C).

The climate at San Fili, like in most of Calabria, is Mediterranean (Csa), according to Köppen (1948). Being located on the Eastern side of a ridge, the area is subject to *Staii* conditions with respect to perturbations coming from the Tyrrhenian sea. It is characterized by heavy and frequent Winter rainfall, caused by cold fronts mainly approaching from North-West, and Autumn rains,



determined by cold air masses from North-East. In Spring, rains show lower intensities than in Autumn, whilst strong convective storms are common at the end of Summer.

The average monthly rains recorded at the Montalto Uffugo gauge (the closest to San Fili) are listed in Table 2. From October to March (i.e. the wet semester), 77% of the annual rainfall is totalized in about 77 rainy days and 36% is recorded in 38 days, during the three wettest months; finally, from June to August (i.e. the three driest months), 6% of the annual rains fall in 11 days.

The Uncino landslide is located at the western margin of San Fili (Fig. 8). **The rock slide is of medium-size (maximum width = 200 m, length > 650 m, estimated maximum vertical depth = 25 m), with a deep-seatedness factor (sensu Hutchinson, 1995) that may be classified as “intermediate”.** It involves Late Miocene conglomerate, arenite and marly clay overlaying Palaeozoic gneiss and biotitic schist. The slope movement repeatedly affected the village, damaging the railway and the local road network, in addition to some buildings: the ancientmost known activation dates back to the beginning of the XX Century (Sorriso-Valvo et al., 1996); from 1960 to 1990, a set of 7 dates of mobilization are listed in Table 3. On such events, the railroad connecting Cosenza to Paola was damaged or even interrupted. Note that, having not been recorded by landslide experts, such type of information is usually affected by intrinsic uncertainty (e.g. concerning the dates of activity) and may be related to either partial or total activations of the phenomenon, with unavoidable problems of homogeneity of the set employed for model calibration. By the way, on 28 April 1987, the railway was put out of service, hence the relevance of the infrastructure decreased, together with media attention.

The informative content of the Uncino case study is quite high, and allows for a more accurate calibration of the kernel with respect to the Sorrento Peninsula case: consequently, a smaller family of optimal solutions are expected. Nevertheless, the known activations still suffer from uncertainties related to dates and affected volumes.

Cumulated antecedent rains, corresponding to the Uncino landslide occurrences, are shown in Fig. 9. Rainfall data were extracted from the records of the nearest rain gauge, located at Montalto Uffugo (cf. Fig. 8). The trends of antecedent rains may be distinguished into 3 main patterns: the curve 2 shows a constant increase of rainfall in time, totalizing the greatest amounts from ca. 90 to 180 days. On the other hand, the case 0 shows the lowest values throughout the considered accumulation period. The curves 1, 3, 4, and 5 totalize intermediate values, with abrupt increases shown by 3 and 5 from 120 to 180 days. Finally, the case 6 looks similar to case 2 between 30 and 90 days, but shows no more increases in the remaining period (analogously to 1 and 4).

The curve 0 does not highlight significant amounts of rainfall in the 30-180 days preceding the landslide activation: for this reason, the occurrence recorded on 23 November 1988 was excluded from the hydrological analysis. Of the remaining curves, case 1 generally shows the lowest amounts from ca. 40 to 180 days.

As a result, the dates of activation from #1 to #5 were selected for calibration, whilst #6 was employed for validation. As a **medium-size** landslide was being considered, the rainfall period employed for calibration spans from 1 September 1959 to 31 August 1980; for validation, it ranges from 1 September 1980 to 31 March 1981 - i.e. including the validation date by ca.  $\pm t_b$  (this latter as obtained from calibration).

## 5 RESULTS

<sup>GA</sup>SAKe was applied to shallow-landslide occurrences in the Sorrento Peninsula and to a **medium-size** slope movement at San Fili, by considering the dates of activation and the daily rainfall series mentioned in section §4.1 and §4.2, and adopting the values of parameters listed in Table 4. As several kernels, among those obtained from calibration, usually allow obtaining similar fitness values, “average kernels” were computed for the considered case studies, by averaging the best 100 kernels.

### 5.1 Application to shallow landslides in the Sorrento Peninsula

In Table 5, the statistics related to the family of optimal kernels (made of the best 100 filter functions, as obtained from calibration) are summarized. From such values, a low variability of  $\Phi$ ,  $t_b$  and  $\mu_0$  can be appreciated;  $\Delta z_{cr}$  shows instead a greater range of values. The average kernel for the Sorrento Peninsula case study is shown in Figure 10: it is characterized by fitness = 0.806, with  $\Delta z_{cr} = 0.00282$ , and  $t_b = 28$  days. From such kernel, antecedent rainfall mostly affecting landslide instability range from 1 to 12 days, and subordinately from 25 to 26 days. Negligible weights refer to rains occurred in the remaining period.

In Fig. 11, the mobility function related to the average kernel is shown. In this case, 4 out of 10 dates of landslide activation are well captured by the model (being ranked at the first 7 positions of the mobility function maxima); the remaining 6 dates do also correspond to relative maxima of the function, but are ranked from the 43<sup>rd</sup> to the 151<sup>st</sup> position. When considering the remaining relative maxima, several false positives can be recognized, mainly up to 1979.

During calibration, the best fitness ( $\Phi=0.807$ ) was first reached after 1749 iterations (at 6<sup>th</sup> individual), with  $\Delta z_{cr} = 0.00441$  and  $t_b = 26$  days. The kernel corresponding to such individual looks similar to the best one in terms of  $t_b$ ,  $\Delta z_{cr}$ , and  $\mu_0$  (Fig. 12). The pattern of the best kernel is only slightly dissimilar from the average one: significant weights can in fact be appreciated up to 14 days, and then between 20-22 and 25-26 days.

By applying the average kernel, a validation was performed against the remaining date of activation (cf. Table 1, #11, multiple event occurred on 10 January 1997). Validation resulted fully satisfied, as shown in Fig. 13: the value of the mobilization function for the event #11, in fact, is well above the  $z_{cr}$  threshold (49.01 vs. 18.05), and is ranked as II highest value among the function maxima (Fig. 13a). The same peak can also be appreciated as the maximum of the period  $\pm t_b$  (Fig. 13b). Accordingly, if adopting the average kernel, the event #11 of landslide activation could properly be predicted by the model.

### 5.2 Application to the Uncino landslide

In Table 6, the statistics related to the family of optimal kernels are summarized. From such values, a low variability of  $t_b$  and  $\Delta z_{cr}$  can be appreciated. The average kernel for the Uncino case study is shown in Fig. 14.

The average kernel is characterized by fitness = 1,  $\Delta z_{cr} = 0.0644$ , and  $t_b = 66$  days. Based on such kernel, antecedent rains from 1 to 17 days, and from 27 to 45 days, mainly affect landslide instability. Relatively smaller weights pertain to the rains occurred more than 53 days before the triggering; for periods older than 66 days, the weights are negligible.

In Fig. 15, the mobility function related to the average kernel highlights that all the 5 dates of activation are well captured by the model (they are ranked at the first 5 positions among the function maxima). When considering the remaining relative maxima of the function, only 4 of them evidence quasi-critical situations (between 1965 and 1966, and subordinately in 1970 and 1977).

During calibration, the best fitness ( $\Phi=1$ ) was first reached after 684 iterations (at 13<sup>th</sup> individual) with  $\Delta z_{cr} = 0.0595$ . The best kernel (Fig. 16) was obtained at iteration 993, at 8<sup>th</sup> individual, with  $\Delta z_{cr} = 0.0631$ . Its pattern results very similar to the average one, with a  $t_b$  of 66 days.

By applying the average kernel, a validation was performed against the last known date of activation (cf. Table 3, #6, occurred on December 1980). Validation resulted fully satisfied, as shown in Fig. 17: the value of the mobilization function for the event #6, in fact, is well above the  $z_{cr}$  threshold (17.49 vs. 16.87), and is ranked as the sixth highest value among the function maxima (Fig. 17a). The same peak can be appreciated as the maximum of the period  $\pm t_b$  (Fig. 17b). Accordingly, if adopting the average kernel, the event #6 could properly be predicted by the model.

## 6 SELF-ADAPTIVE PROCEDURE AND SENSITIVITY ANALYSES

The capability of the model **to react and self-adapt to input changes, like new dates of landslide activation**, was evaluated by a progressive, self-adaptive procedure of calibration and validation, using the information available for the Uncino case study. **To simulate the adoption of <sup>GA</sup>SAKe in a landslide warning system**, the model was iteratively calibrated by the first 2, 3, 4, and 5 dates of activation ( $L$ ), and validated against the remaining 4, 3, 2, 1 dates, respectively. In each experiment, the GA-parameters listed in Table 4 were adopted. Finally, the model was merely calibrated by considering all the 6 dates of activation. The results of the self-adaptive procedure are listed in Table 7. The related kernels are shown in Fig. 18. As a result, a progressive increase in fitness and predictive ability ( $\Delta z_{cr}$ ), together with the base time (ranging from 30 to 80 days), can be appreciated when employing a greater number of dates of activation.

Furthermore, aiming at evaluating the sensitivity of the model with respect to the GA parameters, a series of analyses was performed by considering the Uncino case study. More in detail, the experiments carried out are listed in Table 8. Each simulation stopped after 1500 iterations: GA-parameters were initialized by considering the “benchmark experiment” (cf. values in Table 4), except for the parameter that was in turn varied as indicated in Table 8.

By varying the GA parameters listed in Table 8, the maximum fitness ( $\Phi_{max}$ ), the safety margin ( $\Delta z_{cr}$ ), the number ( $n_i$ ) of iterations needed to first reach  $\Phi_{max}$ , and the base time ( $t_b$ ) of the average kernel are shown in Fig. 19. If experiments with  $\Phi_{max} = 1$  are only taken into account, the minimum and maximum numbers ( $min\_A$ ,  $max\_A$ ) of GA-iterations needed to reach  $\Phi_{max}$ , the minimum and maximum base times ( $min\_t_b$ ,  $max\_t_b$ ) of the average kernel, and the minimum and maximum safety margins ( $min\_ \Delta z_{cr}$ ,  $max\_ \Delta z_{cr}$ ) of the average kernel are listed in Tables 9, 10 and 11.

## 7 DISCUSSION E CONCLUSIONS

In the present paper, the model <sup>GA</sup>SAKe is presented with examples of application to shallow-landslides in Sorrento Peninsula (Campania), and to the **medium-size** Uncino landslide at San Fili (Calabria). Furthermore, the capability of the model to simulate the occurrence of known landslide activations was evaluated by a progressive, self-adaptive procedure of calibration and validation against the Uncino case study. Finally, the sensitivity of the model with respect to the GA parameters was analysed by a series of experiments, performed again by considering the latter landslide.

As concerns the Sorrento Peninsula case study, the maximum fitness obtained during calibration is smaller than unity. For the best 100 kernels,  $\Phi_{max}$ ,  $\Delta z_{cr}$  and  $t_b$  vary in a small range (ca. 0.1%, 4.8%, and 13%, respectively). Furthermore, as mentioned above, for specific types of application (e.g. civil protection), the observed small values of  $\Delta z_{cr}$  would imply short warning times. Consequently,

a suitable kernel should be rather selected by privileging the shortest  $t_b$  or the smallest  $\mu_0$ . In Fig. 12, the four kernels point out that the greatest weights for the first 12-15 days are obtained by selecting the kernel with smallest  $\mu_0$ , thus allowing for the most timely advice if used within an early-warning system.

In the average kernel, the greatest weight can be attributable to the first 12 days, with a maximum base time of about 4 weeks, reflecting the general shape of the curves in Fig. 7, and in good agreement with the shallow type of slope instability considered.

Furthermore, the validation of the average kernel is satisfactory, as the validation date (#11 in Table 1) corresponds to the second highest peak of the mobility function. In addition, no missing alarms and only four false alarms in about 5 years are to be found (i.e. in the period from the last date used for calibration to the one for validation). The peaks of the mobility function corresponding to the activation dates can roughly be grouped in two sets, characterized by distinct values: a first set, with  $z(t) > 40$ , generally includes the ancientmost plus the validation dates (#1, #2, #4, #5, #6, and #11); a second set (#3, #7, #8, #9, and #10), with  $18 < z(t) < 25$ . False alarms result more frequent and higher in the first period (from 1963 to 1980), presumably due to lack of information on landslide activations.

Regarding the Uncino case study, the maximum fitness in calibration reaches unity. With respect to the Sorrento Peninsula case study,  $\Delta z_{cr}$  and  $t_b$  of the best 100 kernels vary in a greater range (ca. 25%, and 30.5%, respectively), with  $\Delta z_{cr}$  one order of magnitude greater. In this case, the kernel would in fact allow for a safety margin of ca. 5%.

In the average kernel, three main periods can be recognized with heavier weights, attributable to *i*) the first 17 days, *ii*) 27-45 days, and *iii*) 54-58 days. The base time ranges from about 8 to 12 weeks, in good agreement with the **medium-size** type of slope instability considered.

Furthermore, the validation of the average kernel performed successfully: in fact, the validation date (#6 in Table 3) corresponds to the third highest peak of the mobility function; even in this case, neither missing alarms nor false alarms in about 2 years (from the last date calibration date to the validation one) are to be found. The peaks of the mobility function corresponding to the activation dates are characterized by  $z(t) > 18$ .

In the self-adaptive procedure applied to the same Uncino case study, values for  $L=6$  merely refer to calibration, whilst the ones for  $2 \leq L \leq 5$  concern validation. With regard to Table 7 and Fig. 20, it can be noticed that:

- for  $2 \leq L \leq 5$ ,  $t_b$  increases 2.7 times with  $L$ , and then remains constant for  $L \geq 5$ ;
- from  $L=2$  to  $L=4$ ,  $z_{j-min}$  and  $z_{cr}$  slightly decrease, and then abruptly increase for  $L \geq 5$ ;
- for  $L \geq 4$ ,  $\Delta z_{cr}$  monotonically increases 72 times with  $L$  (being almost constant in the 2-4 transition);
- $\Phi_v$  monotonically increases 1.7 times with  $L$ .

As a whole, a satisfying performance is obtained starting from 3 dates (i.e. correct predictions in more than 3 out of 4 times). For  $L=5$ , only one false alarm is observed. Finally, the calibration performed by considering all the 6 dates of activation provided fully satisfying results. **Accordingly, the results of the progressive procedure underlined how  $G^A SAKe$  can easily self-adapt to external changes by optimizing its performances, providing increasing fitness values.**

The average kernels obtained by considering from 2 to 6 dates of landslide activation point out increasing base times, with significant weights for the ancientmost rains of the temporal range (Fig.

18). Such results is in good accordance with the extent of the slope movement and, therefore, with the expected prolonged travel times of the groundwater affecting landslide activation.

In the sensitivity analyses, again performed by considering the Uncino landslide,  $\Phi_{max} = 1$  was obtained in 60% of the experiments (cf. Table 8). The results, shown in Fig. 19, and listed in Tables 9, 10, and 11, permit to select the set of parameters that allow for faster GA performances. More in detail:

- a ratio between the number of elitist individuals and the whole population of  $n_e/N=10/20$  or  $8/15$  allow for the fastest GA performances ( $min\_A_i \sim 41\%$  of the reference value). Nevertheless, for increasing both  $n_e$  and  $N$ , this effect seems to vanish (e.g.  $n_e/N=12/25$ ).
- with respect to the benchmark experiment, the explored changes in  $p_c, p_m, p_{mh1}, p_{me},$  and  $p_{mtb}$  do not substantially affect the GA performances with respect to  $min\_A_i$ .
- with respect to the benchmark experiment, the explored changes of parameters determine variation of  $t_b$  from 66 to 219%.
- in case of civil protection applications, the combination of parameters with  $p_{mh1}=55$  allows for activating early-warning procedures with the greatest advance.
- concerning  $max\_ \Delta z_{cr}$ , the best result (increase by 10 times) is obtained when reducing  $N$  to 15.

The calibration experiments discussed in this paper were performed on a standard PC platform (CPU 3 GHz, RAM 4 GB, standalone system SQL and application process). For the study cases of Sorrento Peninsula and Uncino landslide, 2.5 and 1.1 GA-iterations were respectively performed per minute, reaching  $\Phi_{max}$  in 11<sup>h</sup>40<sup>m</sup> and 10<sup>h</sup>20<sup>m</sup>. Depending on availability of High-Performance Computing Clusters, the mentioned durations may strongly be reduced, thus allowing for prompt Civil Protection applications, e.g. based on short-term weather forecasts. By the way, the time needed to calibrate the model can profitably be shortened by properly initializing the kernel, based on expected characteristics of the phenomena under consideration (e.g. the range of  $t_b$  strongly depends on landslide size).

In this study, a 2-steps efficiency criterion was employed: the relative position of the peaks of the mobility function with respect to the dates of landslide activation was first considered, and the fitness computed. Based on the value of  $\Delta z_{cr}$ , the obtained solutions were further ranked. Average, synthetic filter functions can then be computed by selecting the best 100 kernels for successive validation purposes. Alternative metrics (cf., among the others, Krause et al., 2005) for the fitness function are being tested. However, due to uncertainties concerning input data (i.e. rainfall and dates of landslide activation), the adoption of sophisticated techniques does not sound very promising. In addition, problems of over-fitting may depend on both data uncertainties and number of parameters. Commonly, kernels characterized by a complex pattern (and then by many parameters) are needed for simulating groundwater dynamics (Pinault et al., 2001). Nevertheless, more complex kernels do not necessarily imply higher predictive uncertainties (Fienen et al., 2010; Long, 2015). Still, the adopted discrete approach allows focusing only on the timing of the peaks of the mobility function, thus somehow relieving the computational effort. Due to the cited uncertainties in input data, a “temporal window” was in fact employed to help matching dates of activation with the peaks of the mobility function. Further attempts of defining the fitness function by different metrics, and the analysis of its effects on calibration and validation, are being considered against another case study (San Benedetto Ullano, in Calabria, Southern Italy), whose mobility phases have been recently monitored by the same authors (Iovine et al., 2010; Capparelli et al., 2012).

As mentioned above, model calibration may be hampered by either quality or completeness of input data. Commonly, missing dates of activation (mainly in remote periods or in isolated areas) and unsuitability of the rain gauge network (e.g. due to excessive distance of gauges from the landslides) negatively affect model results. Depending on availability of new dates of activation, stemming from further mobilizations or improvement of historical investigations, the predictive capability of the model can be increased through additional calibrations, hence providing new families of optimal solutions, constituted by fewer, higher-significance kernels.

The above considerations suggest an indirect link between the model – despite empirical in type – and the physical characteristics of the slope movements (e.g. dimensions, permeability, initial water content of the slope, length of subsurface water paths). In general, to select the kernel to be applied, it is rather preferable to consider a set of optimal kernels or the average one, instead of a single solution.

Further efforts are in progress to improve the model and its chances of practical application, mainly concerning the implementation of different GA techniques of optimization (in addition to the elitist here employed), the parallelization of the model, and the adoption of a Genetic Programming approach. Finally, through the analytical study of the optimal kernels, a mathematical formulation of discrete filter functions is presently being attempted, aiming at synthesizing optimal and average kernels for an easier comparison with the results of other models available in literature.

## **8 CODE AVAILABILITY**

The release <sup>GA</sup>SAKe of the Self-Adapting Kernel model, discussed in this paper, has been developed by scientists working at CNR-IRPI under Microsoft Windows and Visual Studio integrated development environment. The above release can be requested by the public to the corresponding author of the paper, together with examples of input data and technical support (a user manual is not available yet, but it should be released soon). The model is presently undergoing further refinements and developments, mainly concerning types of GA-selection techniques, the post-processing of results in terms of continuous analytical functions, and the implementation of a library of case studies. Authors are willing to cooperate with external users to further improving the model through applications to case studies from different geo-environmental contexts.

## **ACKNOWLEDGEMENTS**

For the rainfall series of the Calabrian rain gauges, we are grateful to: *Regione Calabria*, Ing. Raffaele Niccoli, *Direttore del Centro Funzionale Multirischi dell'ARPACal*.

For the rainfall series of the Campanian rain gauges, we are grateful to: *Regione Campania*, Ing. Generoso Schiavone, *Dirigente del Settore "Programmazione Interventi di Protezione Civile sul Territorio"*, and Ing. Mauro Biafore, *Dirigente del Servizio 04, Responsabile CFD "Centro funzionale per la previsione meteorologica e il monitoraggio meteo-idro-pluviometrico e delle frane"*.

Finally, we thank the editors and two anonymous reviewers for their constructive comments and insights that allowed us to considerably improve our manuscript.

## **REFERENCES**

- Aleotti, P.: A warning system for rainfall-induced shallow failures, *Eng. Geol.*, 73, 247–265, 2004.  
Alfieri, L., Salamon, P., Pappenberger, F., Wetterhall, F., and Thielen, J.: Operational early warning systems for water-related hazards in Europe, *Environ. Sci. Policy*, 21, 35–49, 2012.

- Amodio-Morelli, L., Bonardi, G., Colonna, V., Dietrich, D., Giunta, G., Ippolito, F., Liguori, V., Lorenzoni, S., Paglionico, A., Perrone, V., Piccarreta, G., Russo, M., Scandone, P., Zanettin Lorenzoni, E., and Zuppetta, A.: L'arco calabro-peloritano nell'orogene appenninico-maghrebide, *Mem. Soc. Geol. Ital.*, 17, 1–60, 1976 (in Italian).
- AMRA: Overview of intense rainfall on volcanic soils—regional and local scale, in: *SafeLand - Living with landslide risk in Europe: Assessment, effects of global change, and risk management strategies*, edited by: Crosta, G.B., Agliardi, F., Frattini, P., Sosio, R., 101–122. 2012.
- Berti, M., Martina, M.L.V., Franceschini, S., Pignone, S., Simoni, A., and Pizziolo, M.: Probabilistic rainfall thresholds for landslide occurrence using a Bayesian approach, *J. Geophys. Res.*, 117, F04006, <http://dx.doi.org/10.1029/2012JF002367>, 2012.
- Brand, E.W., Premchitt, J., and Phillipson, H.B.: Relationship between rainfall and landslides, in: *Proceedings of the 4<sup>th</sup> International Symposium on Landslides*, Toronto, vol. 1, BiTech Publishers, Vancouver, Canada, 377–384. 1984.
- Brunetti, M.T., Peruccacci, S., Rossi, M., Luciani, S., Valigi, D. and Guzzetti, F.: Rainfall thresholds for the possible occurrence of landslides in Italy, *Nat. Hazards Earth Syst. Sci.*, 10, 447–458, 2010.
- Brunsdon, D.: Mudslides, in: *Slope Instability*, edited by Brunsdon, D., and Prior, D.B., John Wiley & Sons, London, 363–418, 1984.
- Caine, N.: The rainfall intensity-duration control of shallow landslides and debris flows, *Geografiska Annal*, 62A, 23–27, 1980.
- Calcaterra, D., and Santo, A.: The January 10, 1997 Pozzano landslide, Sorrento Peninsula, Italy, *Eng. Geol.*, 75, 181–200, 2004.
- Campbell, R.H.: Debris flow originating from soil slip during rainstorm in southern California, *Q. J. Eng. Geol.*, 7, 377–384, 1975.
- Cannon, S.H., and Ellen, S.D.: Rainfall conditions for abundant debris avalanches, San Francisco Bay region, California, *California Geology*, 38 (12), 267–272, 1985.
- Capparelli, G., and Versace, P.: FLAIR and SUSHI: two mathematical models for early warning of landslides induced by rainfall, *Landslides*, 8, 67–79, 2011.
- Capparelli, G., Iaquina, P., Iovine, G., Terranova, O.G., and Versace P.: Modelling the rainfall-induced mobilization of a large slope movement in northern Calabria, *Nat. Hazards*, 61(1), 247–256, 2012.
- Carter, J.: The notion of Threshold: an investigation into conceptual accompaniment in Aristotle and Hegel, *Conserveries mémorielles*, 7, available at: <http://cm.revues.org/431>, last access: 10 December 2014, 2010.
- Cascini, L., and Versace, P.: Eventi pluviometrici e movimenti franosi, in: *Atti del XVI Convegno Nazionale di Geotecnica*, Bologna, Italy, 14–16 may 1986, 171–184, 1986 (in Italian).
- Cascini, L., and Versace, P.: Relationship between rainfall and landslide in a gneissic cover, in: *Proceedings of the 5<sup>th</sup> International Symposium on Landslides*, Lausanne, Switzerland, 565–570, 1988.
- Cascini, L., Sorbino, G., Cuomo, S., Ferlisi, S.: Seasonal effects of rainfall on the shallow pyroclastic deposits of the Campania region (southern Italy), *Landslides*, 11, 779–792, 2014.
- CASMEZ: Carta Geologica della Calabria, F.229IINE “Montalto Uffugo” (in scale 1:25000), Poligrafica & CarteValori, Ercolano, Napoli, Italy, 1967 (in Italian).

- Cauvin, S., Cordier, M.-O., Dousson, C., Laborie, P., Lévy, F., Montmain, J., Porcheron, M., Servet, I., and Travé-Massuyès, L.: Monitoring and alarm interpretation in industrial environments, *AI Commun.*, 11 (3-4), 139-173, 1998.
- Chow, V.T., Maidment, D.R., and Mays, L.W.: *Applied Hydrology*, Mc Graw Hill, New York, USA, 572 pp., 1988.
- Corominas, J.: Landslides and climate, Keynote lecture, in: *Proceedings of the 8th International Symposium on Landslides*, vol. 4, Cardiff, United Kingdom, 26-30 June 2000, 1-33, 2000.
- Crosta, G.B.: Regionalization of rainfall thresholds: an aid to landslide hazard evaluation, *Environ. Geol.*, 35 (2-3), 131-145, 1998.
- Crosta, G.B., Dal Negro, P., and Frattini, P.: Soil slips and debris flows on terraced slopes, *Nat. Hazards Earth Syst. Sci.*, 3, 31-42, 2003.
- Crozier, M.J.: The climate-landslide couple: a southern hemisphere perspective, in: *Rapid mass movement as a source of climatic evidence for the Holocene*, edited by: Matthews, J.A., Brunsdon, D., Frenzel, B., Gläser, B., and Weiß, M.M., Gustav Fischer, Stuttgart, 333-354, 1997.
- Cuomo, S. and Della Sala, M.: Rainfall-induced infiltration, runoff and failure in steep unsaturated shallow soil deposits, *Eng. Geol.*, 162, 118-127, 2013.**
- D'Ambrosio, D., Spataro, W., and Iovine, G.: Parallel genetic algorithms for optimising cellular automata models of natural complex phenomena: an application to debris-flows, *Computer and Geosciences*, 32, 861-875, 2006.
- De Jong, K.A.: *An analysis of the behavior of a class of genetic adaptive systems*, Ph.D. dissertation, Department of Computer and Communication Sciences, University of Michigan, Ann Arbor, USA, 1975.
- Del Prete, M., Guadagno, F.M., and Hawkins, A.B.: Preliminary report on the landslides of 5 May 1998, Campania, southern Italy, *Bull. Eng. Geol. Env.*, 57, 113-129, 1998.
- Di Crescenzo, G., and Santo, A.: Analisi morfologica delle frane da scorrimento-colata rapida in depositi piroclastici della Penisola Sorrentina (Campania), *Geografia Fisica e Dinamica Quaternaria*, 22, 57-72, 1999 (in Italian).
- Di Crescenzo, G., and Santo, A.: Debris slides-rapid earth flows in the carbonate massifs of the Campania region (Southern Italy): morphological and morphometric data for evaluating triggering susceptibility, *Geomorphology*, 66, 255-276, 2005.
- Dikau, R., and Schrott, L.: The temporal stability and activity of landslides in Europe with respect to climatic change (TESLEC): main objectives and results, *Geomorphology*, 30 (1-2), 1-12, 1999.
- Ducci, D., and Tranfaglia, G.: L'impatto dei cambiamenti climatici sulle risorse idriche sotterranee in Campania, *Geologi. Boll. Ordine Geologi della Campania*, 1-4, 13-21, 2005 (in Italian).
- Ellen, S.D.: Description and mechanics of soil slip/debris flows in the storm, in: *Landslides, floods, and marine effects of the storm of January 3-5, 1982, in the San Francisco Bay region*, California, edited by Ellen, S.D., and Wieczorek, G.F., U.S. Geol. Surv. Prof. Pap., 1434, 63-112, 1988.
- Fienen, M.N., Doherty, J.E., Hunt, R.J., and Reeves, H.W.: Using prediction uncertainty analysis to design hydrologic monitoring networks: example applications from the Great Lakes water availability pilot project, US Geol. Surv., Reston Virginia, Scientific Investigations Report 2010-5159, 44 pp., 2010.**



- Fiorillo, F., and Wilson, R.: Rainfall induced debris flows in pyroclastic deposits, Campania (southern Italy), *Eng. Geol.*, 75, 263–289, 2004.
- Gariano, S.L., Brunetti, M.T., Iovine, G., Melillo, M., Peruccacci, S., Terranova, O., Vennari, C., and Guzzetti, F.: Calibration and validation of rainfall thresholds for shallow landslide forecasting in Sicily, southern Italy, *Geomorphology*, 228, 653–665, 2015.
- Goldberg, D.E.: *Genetic Algorithms in Search, Optimization and Machine Learning*, Addison-Wesley, Boston, USA, 1989.
- Gullà, G., Aceto, L., Antronico, L., Cilento, M., Niceforo, D., Perna, E., and Terranova, O.: Failure and post failure conditions of a landslide involving weathered and degraded rocks, in *Proceedings of the IX International Symposium on Landslide, Rio de Janeiro, Brazil, 28 June - 2 July 2004*, 1241–1245, 2004.
- Guzzetti, F.: Landslide fatalities and evaluation of landslide risk in Italy, *Eng. Geol.*, 58, 89–107, 2000.
- Guzzetti, F., Peruccacci, S., Rossi, M., and Stark, C.P.: Rainfall thresholds for the initiation of landslides in central and southern Europe, *Meteorol. Atmos. Phys.*, 98, 239–267, 2007.
- Guzzetti, F., Peruccacci, S., Rossi, M., and Stark, C.P.: The rainfall intensity-duration control of shallow landslides and debris flow: an update, *Landslides*, 5, 3–17, 2008.
- Hinton, G.E., and Nowlan, S.J.: How learning can guide evolution, *Complex Systems*, 1, 495–502, 1987.
- Holland, J.H.: *Adaptation in Natural and Artificial Systems*. University of Michigan Press, Ann Arbor, USA, 1975.
- Hutchinson, J.N.: Deep-seated mass movements on slopes, *Mem. Soc. Geol. It.*, 50, 147–164, 1995.**
- Iovine, G., D'Ambrosio, D., and Di Gregorio, S.: Applying genetic algorithms for calibrating a hexagonal cellular automata model for the simulation of debris flows characterised by strong inertial effects, *Geomorphology*, 66, 287–303, 2005.
- Iovine, G., Iaquina, P., and Terranova, O.: Emergency management of landslide risk during Autumn-Winter 2008/2009 in Calabria (Italy). The example of San Benedetto Ullano, in: *Proceedings of the 18<sup>th</sup> World IMACS Congress and MODSIM09 International Congress on Modelling and Simulation*, Modelling and Simulation Society of Australia and New Zealand and International Association for Mathematics and Computers in Simulation, July 2009, 2686–2693, 2009.
- Iovine, G., Lollino, P., Gariano, S.L., and Terranova, O.G.: Coupling limit equilibrium analyses and real-time monitoring to refine a landslide surveillance system in Calabria (southern Italy), *Nat. Hazards Earth Syst. Sci.*, 10, 2341–2354, 2010.**
- Jakob, M., and Weatherly, H.: A hydroclimatic threshold for landslide initiation on the North Shore Mountains of Vancouver, British Columbia, *Geomorphology*, 54, 3–4, 137–156, 2003.
- Keefer, D.K., Wilson, R.C., Mark, R.K., Brabb, E.E., Brown III W.M., Ellen S.D., Harp E.L., Wiczorek G.F., Alger C.S., and Zatkan, R.S.: Real-Time Landslide Warning During Heavy Rainfall, *Science*, 238 (4829), 921–925, 1987.
- Köppen, W.: *Climatologia, con un estudio de los climas de la tierra*, Fondo de Cultura Economica, Mexico, 479 pp., 1948.
- Krause, P., Boyle D.P., and Bäse, F.: Comparison of different efficiency criteria for hydrological model assessment, *Adv. Geosciences*, 5, 89–97, 2005**
- Lanzafame, G., and Mercuri, T.: Interruzioni ferroviarie in Calabria conseguenti a fenomeni naturali (1950-1973), *Geodata*, 3, Cosenza, Italy, 46 pp., 1975 (in Italian).

- Long, A.J.: RRAWFLOW: Rainfall-Response Aquifer and Watershed Flow Model (v1.15), *Geosci. Model Dev.*, 8, 865–880, 2015.
- Marques R., Zêzere J., Trigo R., Gaspar J., and Trigo, I.: Rainfall patterns and critical values associated with landslides in Povoação County (São Miguel Island, Azores): relationships with the North Atlantic Oscillation, *Hydrol. Process.*, 22(4), 478–494, 2008.
- Mele, R., and Del Prete, S.: Lo studio della franosità storica come utile strumento per la valutazione della pericolosità da frane. Un esempio nell'area di Gragnano (Campania), *Boll. Soc. Geol. Ital.*, 118, 91–111, 1999 (in Italian).
- Mitchell, M.: *An Introduction to Genetic Algorithms*, MIT Press, Cambridge, United Kingdom, 1996.
- Monaco, C., and Tortorici, L.: Active faulting in the Calabrian arc and eastern Sicily, *J. Geodyn.*, 29, 407–424, 2000.
- Montgomery, D.R., and Dietrich, W.E.: A physically-based model for the topographic control on shallow landsliding, *Water Resour. Res.*, 30, 1153–1171, 1994.
- Nolfi, S., and Marocco, D.: Evolving robots able to integrate sensory-motor information over time, *Theor Biosci*, 120, 287–310, 2001.
- Peres, D.J., and Cancelliere, A.: Derivation and evaluation of landslide-triggering thresholds by a Monte Carlo approach, *Hydrol. Earth Syst. Sci.*, 18, 4913–4931, 2014.
- Petley, D.N.: The global occurrence of fatal landslides in 2007, in: *International Conference on Management of Landslide Hazard in the Asia-Pacific Region*, Tokyo, Japan, 590–600, 2008.
- Pinault, J.-L., Plagnes, V., and Aquilina, L.: Inverse modeling of the hydrological and the hydrochemical behavior of hydrosystems: Characterization of karst system functioning, *Water Resour. Res.*, 37(8), 2191–2204, 2001.
- Pisani, G., Castelli, M., and Scavia, C.: Hydrogeological model and hydraulic behaviour of a large landslide in the Italian Western Alps, *Nat. Hazards Earth Syst. Sci.*, 10, 2391–2406, 2010.
- Poon, P.W., and Parks, G.T.: Optimizing PWR reload core design, *Parallel Solving from Nature*, 2, 371–380, 1992.
- Pradhan, B., and Buchroithner, M.: *Terrigenous Mass Movements: Detection, Modelling, Early Warning and Mitigation Using Geoinformation Technology*, Springer, 400 pp., 2012.
- Rossi, F., and Villani, P. (eds.): *Valutazione delle piene in Campania*, CNR-GNDCI publications, Grafica Metellioana &C., Cava de' Tirreni, Italy, 310 pp., 1994.
- Salvati, P., Bianchi, C., Rossi, M., and Guzzetti, F.: Societal landslide and flood risk in Italy. *Nat. Hazards Earth Syst. Sci.*, 10, 465–483, 2010.
- Sengupta, A., Gupta, S., and Anbarasu, K.: Rainfall thresholds for the initiation of landslide at Lanta Khola in north Sikkim, India, *Nat. Hazards*, 52, 31–42, 2010.
- Servizio Geologico, *Sismico dei Suoli: I numeri delle frane*, Regione Emilia-Romagna Publisher, Bologna, 94 pp., 1999 (in Italian).
- Servizio Idrografico: *Annali Idrologici, Parte I, Compartimento di Napoli*, Istituto poligrafico e Zecca dello Stato, Rome, Italy, 1948-1999.
- Sirangelo, B., and Versace, P.: A real time forecasting for landslides triggered by rainfall, *Meccanica*, 31, 1–13, 1996.
- Sorriso-Valvo, G.M., Agnesi, V., Gulla, G., Merenda, L., Antronico, L., Di Maggio, C., Filice, E., Petrucci, O., and Tansi, C.: Temporal and spatial occurrence of landsliding and correlation with precipitation time series in Montalto Uffugo (Calabria) and Imera (Sicilia) areas, in: *Temporal occurrence and forecasting of landslides in the European Community. Final Report, II*,

- European Community, Programme EPOCH, Contract 90 0025, edited by Casale, R., Fantechi, R., Flageollet, J.C., 825–869, 1994.
- Sorriso-Valvo, G.M., Antronico, L., Catalano, E., Gullà, G., Tansi, C., Dramis, F., Ferrucci, F., and Fantucci, R.: Final Report (June 1996), CNR-IRPI, in: The temporal stability and activity of landslides in Europe with respect to climatic change (TESLEC), Final Report, Part II, edited by: Dikau, R., Schrot, L., Dehn, M., Hennrich, K., and Rasemann, S., 87–152. 1996.
- Terlien, M.T.J.: The determination of statistical and deterministic hydrological landslide-triggering thresholds, *Environ. Geol.*, 35 (2-3), 125–130, 1998.
- Terranova, O.: Caratteristiche degli eventi pluviometrici a scala giornaliera in Calabria, in: XXIX Convegno di Idraulica e Costruzioni Idrauliche, Trento, Italy, 7-10 september 2004, 343–350, 2004 (in Italian).
- Terranova, O., Antronico, L., and Gullà, G.: Pluviometrical events and slope stability on weathered and degraded rocks (Acri, Calabria, Italy), in Proceedings of the IX International Symposium on Landslide, Rio de Janeiro, Brazil, 28 June - 2 July 2004, 335–342, 2004.
- Terranova, O., Iaquina, P., Gariano, S.L., Greco, R., and Iovine, G.: *CM SAKe*: A hydrological model to forecasting landslide activations, in: *Landslide Science and Practice*, vol. 3, edited by: Margottini, C., Canuti, P., and Sassa K., Springer, 73–79, 2013.
- Terzaghi, K.: Stability of steep slopes on hard unweathered rock, *Geotechnique*, 12 (4), 251–270, 1962.
- Trigila, A.: Rapporto sulle frane in Italia. Il Progetto IFFI. Metodologia, risultati e rapporti regionali, APAT, Roma, Italy, 681 pp., 2007 (in Italian).
- Trigo, R.M., Zêzere, J.L., Rodrigues, M.L., and Trigo, I.F.: The influence of the North Atlantic Oscillation on rainfall triggering of Landslides near Lisbon, *Nat. Hazards*, 36 (3), 331–354, 2005.
- UNDRO: Mitigating Natural Disasters. Phenomena, Effects and Options, United Nations, New York, USA, 164 pp., 1991.
- Van Asch, Th.V.J., Buma, J., and Van Beek, L.P.H.: A view on some hydrological triggering systems in landslides, *Geomorphology*, 30 (1-2), 25–32, 1999.
- Vennari, C., Gariano, S.L., Antronico, L., Brunetti, M.T., Iovine, G., Peruccacci, S., Terranova, O., and Guzzetti, F.: Rainfall thresholds for shallow landslide occurrence in Calabria, southern Italy, *Nat. Hazards Earth Syst. Sci.*, 14, 317–330, 2014.
- White, I.D., Mottershead, D.N., and Harrison, J.J.: *Environmental Systems*, 2<sup>nd</sup> Edition, Chapman & Hall, London, United Kingdom, 616 pp., 1996.
- Wieczorek, G.F.: Effect of rainfall intensity and duration on debris flows in central Santa Cruz Mountains, California, in: *Debris Flows/Avalanches: Processes, Recognition and Mitigation*, edited by: Costa, J.E., and Wieczorek GF, Geological Society of America, *Reviews in Engineering Geology* 7, 93–104. 1987
- Wieczorek, G.F., and Glade, T.: Climatic factors influencing occurrence of debris flows, in: *Debris flow hazards and related phenomena*, edited by: Jakob, M. and Hungr, O., Berlin Heidelberg, Springer, 325–362, 2005.
- Wilson, R.C., and Wieczorek, G.F.: Rainfall thresholds for the initiation of debris flow at La Honda, California, *Environ. Eng. Geosci.*, 1, 11–27, 1995.
- Zêzere, J.L., and Rodrigues, M.L.: Rainfall thresholds for landsliding in Lisbon area (Portugal), in *Landslides*, edited by: Rybar, J, Stemberk, J, and Wagner, P., A.A. Balkema, Lisse, The Netherlands, 333–338, 2002.

**Table 1.** Dates of activation of the shallow landslides in the Sorrento Peninsula. Key: date = day of occurrence; type = widespread (multiple) or few (single) activation; site = municipality including the affected location; period employed = dates used for calibration (except for #11); rank = relative position of the corresponding maximum of the mobility function obtained by calibration. An asterisk marks the date employed for validation. In Italics, the activation date (#0) excluded due to hydrological constraints.

#	Date	type	site	reference	period employed	rank
1	17 February 1963	multiple; single	Gragnano, Pimonte; Castellammare	Del Prete et al. 1998	17 Feb 1963	17 Feb 1963 (1)
2	23 November 1966	single	Vico Equense (Scrajo), Arola, Ticciano	Del Prete et al. 1998	23 Nov 1966	24 Nov 1966 (4)
0	<i>14 April 1967</i>	<i>single</i>	<i>Castellammare (Pozzano)</i>	<i>Del Prete et al. 1998; AMRA, 2012</i>	-	-
3	15 March 1969; 24 March 1969	multiple; multiple	Cava de' Tirreni, Agerola, Scrajo Seiano	Del Prete et al. 1998; AMRA, 2012	15-24 Mar 1969	25 Mar 1969 (65)
4	02 January 1971	single	Gragnano	Del Prete et al. 1998	02 Jan 1971	3 Jan 1971 (3)
5	21 January 1971	single	Gragnano	Del Prete et al. 1998	21 Jan 1971	21 Jan 1971 (7)
6	04 November 1980	single	Vico Equense (Scrajo)	Del Prete et al. 1998	04 Nov 1980	6 Nov 1980 (94)
7	14 November 1982	single	Pozzano	Del Prete et al. 1998	14 Nov 1982	15 Nov 1982 (151)
8	22 February 1986	multiple	Palma Campania, Castellammare, Vico Equense	Del Prete et al. 1998	22 Feb 1986	24 Feb 1986 (120)
9	23 February 1987	single	Gragnano, Castellammare	Del Prete et al. 1998; AMRA, 2012	23 Feb 1987	23 Feb 1987 (73)
10	23 November 1991	single	Pozzano	Del Prete et al. 1998	23 Nov 1991	24 Nov 1991 (43)
11	10 January 1997	multiple	Pozzano; Castellammare, Nocera, Pagani, Amalfitana Coast	Del Prete et al. 1998 AMRA, 2012	10 Jan 1997	*

**Table 2.** Average monthly rainfall and number of rainy days at the Montalto Uffugo rain gauge (468 m a.s.l.).

	Sep	Oct	Nov	Dec	Jan	Feb	Mar	Apr	May	Jun	Jul	Aug	year
rainfall (mm)	70.4	125.1	187.9	220.8	198.1	160.3	132.8	98.9	64.6	27.8	18.3	28.6	1333.6
rainy days	6.9	10.6	12.8	14.3	14.3	12.5	12.6	10.7	8.26	4.7	2.62	3.84	114.0

**Table 3.** Dates of activation of the Uncino landslide. Periods (instead of singular dates) were considered in case of uncertain timing of activation. Key = #: Identification number of the date (in bold, used for calibration); dates/periods derived from literature; dates/periods employed for calibration or validation; references: sources of information on activation dates; rank: relative position and dates of the maxima of the mobility function during calibration. An asterisk marks the activation employed for validation. In Italics, the activation date (#0) excluded due to hydrological constraints.

#	date	reference	period	rank
<b>1</b>	16, 21 January 1960	Sorriso-Valvo et al., 1996	16-21 Jan 1960	18 Jan 1960 (5)
<b>2</b>	Winter 1963	Sorriso-Valvo et al., 1994	01 Nov 1962 – 14 Apr 1963	29 Mar 1963 (1)
<b>3</b>	15 April 1964 (h 22:00)	Sorriso-Valvo et al., 1994	15 Apr 1964	14 Apr 1964 (3)
<b>4</b>	14 December 1966	Lanzafame and Mercuri, 1975	14 Dec 1966	16 Dec 1966 (2)
<b>5</b>	10-14, 21 February 1979	Sorriso-Valvo et al., 1994	10-21 Feb 1979	15 Feb 1979 (4)
<b>6</b>	December 1980	Sorriso-Valvo et al., 1994	01-31 Dec 1980	*
<i>0</i>	<i>23 November 1988</i>	<i>Sorriso-Valvo et al., 1996</i>	-	-

**Table 4.** Values of the parameters of  $GA_{SAKe}$  adopted in the calibration procedure (benchmark experiment).

<b>symbol</b>	<b>parameter</b>	<b>value</b>
$N$	individuals of each GA population	20
$t_b$	base time (Uncino landslide)	30 ÷ 180 days
$t_b$	base time (shallow landslides in the Sorrento Peninsula)	2 ÷ 30 days
$p_{mh1}$	percentages of the maximum height of the kernel,	50%, 150%
$p_{mh2}$	used to defining the range in which $dh$ is randomly obtained	
$p_c$	probability of crossover	75%
$p_m$	probability of mutation	25%
$p_{me}$	number of mutated elements of the kernel, expressed as a percentage of $t_b$	25%
$p_{mtb}$	factor defining the range in which $dt_b$ is selected	0.2 ÷ 5
$A$	number of GA-iterations (Uncino landslide case study)	5000
$A$	number of GA-iterations (Sorrento Peninsula case study)	3000
$n_e$	number of "elitist" individuals	8

**Table 5.** Sorrento Peninsula case study. Statistics for the best 100 kernels.

	$\Phi$	$\Delta z_{cr}$	$t_b$	$\mu_0$
<b>min</b>	0.806	3.82E-05	26.0	9.460
<b>average</b>	0.806	0.00418	30.4	9.567
<b>max</b>	0.807	0.00801	31.0	10.448
<b>median</b>	0.806	0.00499	31.0	9.567
<b>mode</b>	0.806	0.00499	31.0	9.567
<b>dev. st.</b>	7.65E-05	0.00183	0.862	0.146



**Table 6.** Uncino landslide case study. Statistics for the best 100 kernels.

	$\Delta z_{cr}$	$t_b$
<b>min</b>	0.0524	57.0
<b>average</b>	0.0581	69.5
<b>max</b>	0.0692	82.0
<b>median</b>	0.0581	69.0
<b>mode</b>	0.0558	69.0
<b>dev. st.</b>	0.00373	3.12

**Table 7.** Uncino landslide case study. Results of progressive calibration. Key:  $L$ ,  $t_b$ ,  $z_{j-min}$ ,  $z_{cr}$ ,  $\Delta z_{cr}$ ): model parameters concerning calibration (for explanation, cf. text);  $\Phi_v$ ) fitness obtained by validating the “average kernel”, obtained in calibration, against the 6 dates of activation. In *Italics*, results obtained when calibrating the model by using all the 6 available dates (no validation performed).

$L$	$t_b$	$z_{j-min}$	$z_{cr}$	$\Delta z_{cr}$	$\Phi_v$
2	30	13.93	13.89	0.0029	0.59
3	54	11.05	11.04	0.0009	0.78
4	55	10.21	10.20	0.0010	0.87
5	80	16.44	16.34	0.0061	0.95
<i>6</i>	<i>80</i>	<i>18.63</i>	<i>17.43</i>	0.0644	<i>1.00</i>

**Table 8.** Uncino landslide case study. Values of the parameters adopted in the sensitivity analyses. In bold, the experiments with  $\Phi_{max} = 1$ . Boxes evidence the worst experiment (in Italics), and the best one (underlined).

<i>symbol</i>	<i>values</i>				
$n_e$	<b>6</b>	<i>7</i>	<sup>a)</sup> <b>8</b>	<b>9</b>	<u><b>10</b></u>
$p_c$	60%	67.5%	<sup>a)</sup> <b>75%</b>	<i>82.5%</i>	90%
$p_m$	20%	<b>22.5%</b>	<sup>a)</sup> <b>25%</b>	<b>27.5%</b>	30%
$p_{mh1}$ ,	60%,	<b>55%</b> ,	<sup>a)</sup> <b>50%</b> ,	45%,	40%,
$p_{mh2}$	140%	<b>145%</b>	<sup>a)</sup> <b>150%</b>	155%	160%
$p_{me}$	20%	22.5%	<sup>a)</sup> <b>25%</b>	27.5%	<b>30%</b>
$p_{mtb}$	<b>0.25 ÷ 4</b>	0.22 ÷ 4.5	<sup>a)</sup> <b>0.2 ÷ 5</b>	<b>0.18 ÷ 5.5</b>	0.17 ÷ 6
$N, n_e$		<b>25, 8</b>	<sup>a)</sup> <b>20, 8</b>	<b>15, 8</b>	
$N, n_e$		<b>25, 12</b>	<b>25, 10</b>	<b>25, 8</b>	

<sup>a)</sup> Reference values (i.e., those of the benchmark experiment - cf. Table 4)

**Table 9.** Minimum ( $min_{A_i}$ ) and maximum ( $max_{A_i}$ ) numbers of GA iterations needed to reach  $\Phi_{max}$  (only experiments with  $\Phi_{max} = 1$  are considered). In the first column, the letters refer to Fig. 19. In bold, the best and worst experiments. An asterisk marks the experiment  $e$ , in which  $\Phi_{max}$  was reached only for  $p_c=75$ . In Italics, the combinations of parameters of the benchmark experiment (cf. Table 4).

$\hat{s}$	$N$	<i>parameter</i>	$min_{A_i}$	$max_{A_i}$
<i>a</i>	20	$n_e=8$		<i>684</i>
<b>a</b>	20	$n_e=10$	<b>279</b>	
<i>c</i>	25	$n_e=8$	469	
<i>c</i>	25	$n_e=12$		<b>1477</b>
<i>e</i>	20	$p_c=75$	<i>684*</i>	
<i>g</i>	20	$p_m=25$	<i>684</i>	
<i>g</i>	20	$p_m=27.5$		1086
<i>i</i>	20	$p_{mh1}=50$	<i>684</i>	
<i>i</i>	20	$p_{mh1}=55$		836
<i>k</i>	20	$p_{mc}=25$	<i>684</i>	
<i>k</i>	20	$p_{mc}=30$		996
<i>m</i>	20	$p_{mb}=5$	<i>684</i>	
<i>m</i>	20	$p_{mb}=5.5$		1052
<i>o</i>	15	$n_e=8$	405	

**Table 10.** Minimum ( $min\_t_b$ ) and maximum ( $max\_t_b$ ) base time of the average kernel (only experiments with  $\Phi_{max} = 1$  are considered). In the first column, the letters refer to Fig. 19. In bold, the best and worst experiments. An asterisk marks the experiment  $e$ , in which  $\Phi_{max}$  was reached only for  $p_c=75$ . In Italics, the combinations of parameters of the benchmark experiment (cf. Table 4).

$\hat{S}$	$N$	<i>parameter</i>	<i>min_t_b</i>	<i>max_t_b</i>
<i>a</i>	20	$n_e=8$	<i>66,59</i>	
a	20	$n_e=10$		144,85
c	25	$n_e=8$		132,00
c	25	$n_e=12$	56,17	
<i>e</i>	20	$p_c=75$	<i>66,59*</i>	
<i>g</i>	20	$p_m=25$	<i>66,59</i>	
g	20	$p_m=27.5$		139,20
<i>i</i>	20	$p_{mh1}=50$		<i>66,59</i>
i	20	$p_{mh1}=55$	<b>44,00</b>	
<i>k</i>	20	$p_{mc}=25$	<i>66,59</i>	
k	20	$p_{mc}=30$		<b>146,93</b>
<i>m</i>	20	$p_{mtb}=5$	<i>66,59</i>	
m	20	$p_{mtb}=4$		136,06
o	15	$n_e=8$		145,79

**Table 11.** Minimum ( $\min\_ \Delta z_{cr}$ ) and maximum ( $\max\_ \Delta z_{cr}$ ) safety margin of the average kernel (only experiments with  $\Phi_{max} = 1$  are considered). In the first column, the letters refer to Fig. 19. In bold, the best and worst experiments. An asterisk marks the experiment  $e$ , in which  $\Phi_{max}$  was reached only for  $p_e=75$ . In Italics, the combinations of parameters of the benchmark experiment (cf. Table 4).

$\S$	$N$	<i>parameter</i>	$\min\_ \Delta z_{cr}$	$\max\_ \Delta z_{cr}$
a	20	$n_e=7$		0.007
a	20	$n_e=9$	0.002	
c	25	$n_e=8$		0.014
c	25	$n_e=12$	0.002	
<i>e</i>	20	$p_e=75$	<i>0.005*</i>	
g	20	$p_m=22.5$		0.006
g	20	$p_m=27.5$	<b>0.001</b>	
<i>i</i>	20	$p_{mhi}=50$		<i>0.005</i>
i	20	$p_{mhi}=55$	0.004	
<i>k</i>	20	$p_{me}=25$	<i>0.005</i>	
k	20	$p_{me}=30$		0.006
<i>m</i>	20	$p_{mib}=5$	<i>0.005</i>	
m	20	$p_{mib}=4$		0.009
o	15	$n_e=8$		<b>0.055</b>
<i>o</i>	20	$n_e=8$	<i>0.005</i>	

Figure 1. Scheme of the calibration procedure of the model  $GA^{SAKe}$ .

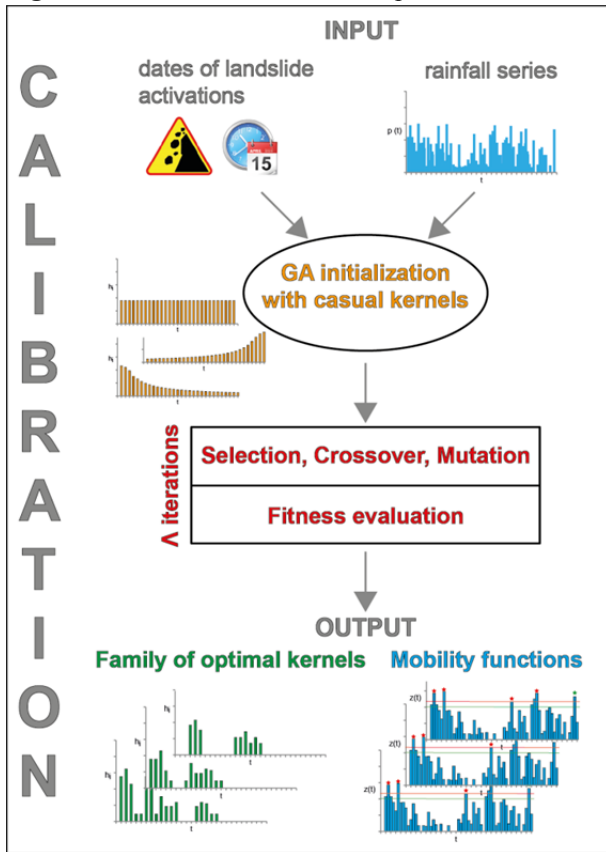
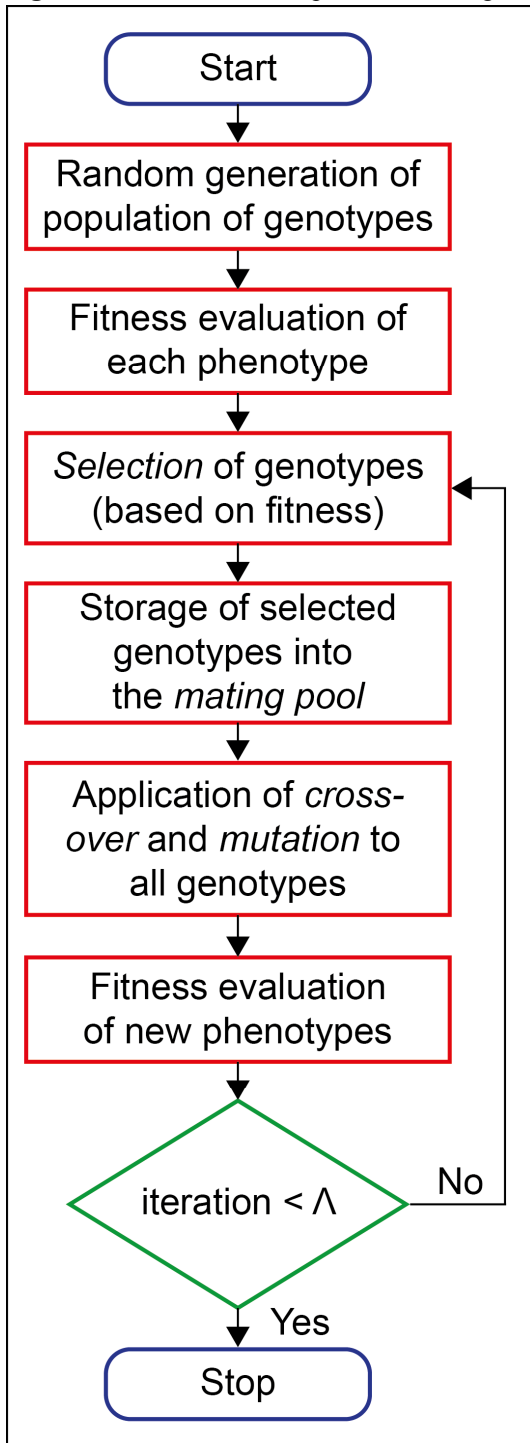
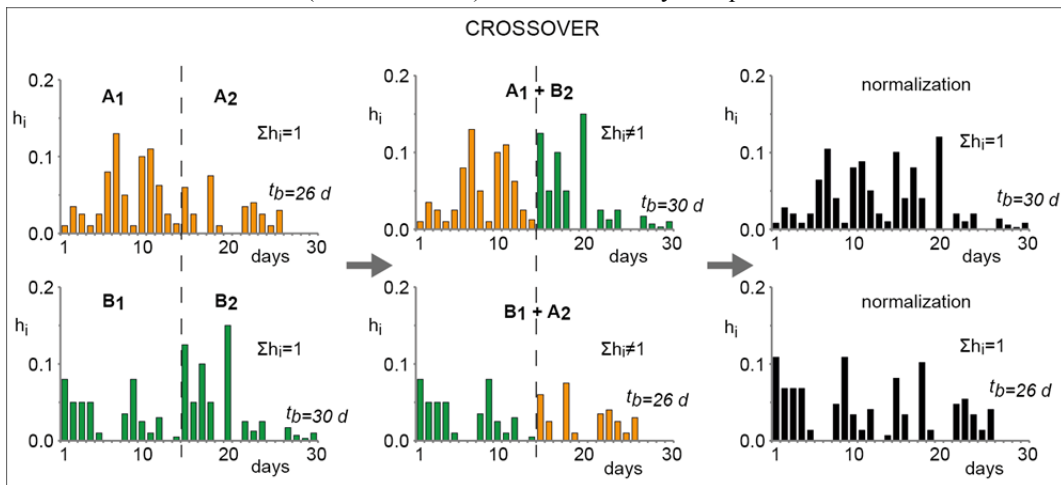


Figure 2. Scheme of the adopted Genetic Algorithm.





**Figure 3.** Example of crossover. The genetic codes of the parents (elements in orange and green) are first mixed; then, the children are normalized (black elements) to ensure validity of equation 2.



**Figure 4.** Examples of mutation. On the left, the genetic code of the parent individual (elements in blue). In the second histogram, mutation is applied to some elements of the parent (in red, added amounts; in grey, subtracted amounts). Then, the base time can either be decreased (upper sequence) or increased (lower sequence). Finally, the children are normalized (black elements) to ensure validity of equation 2.

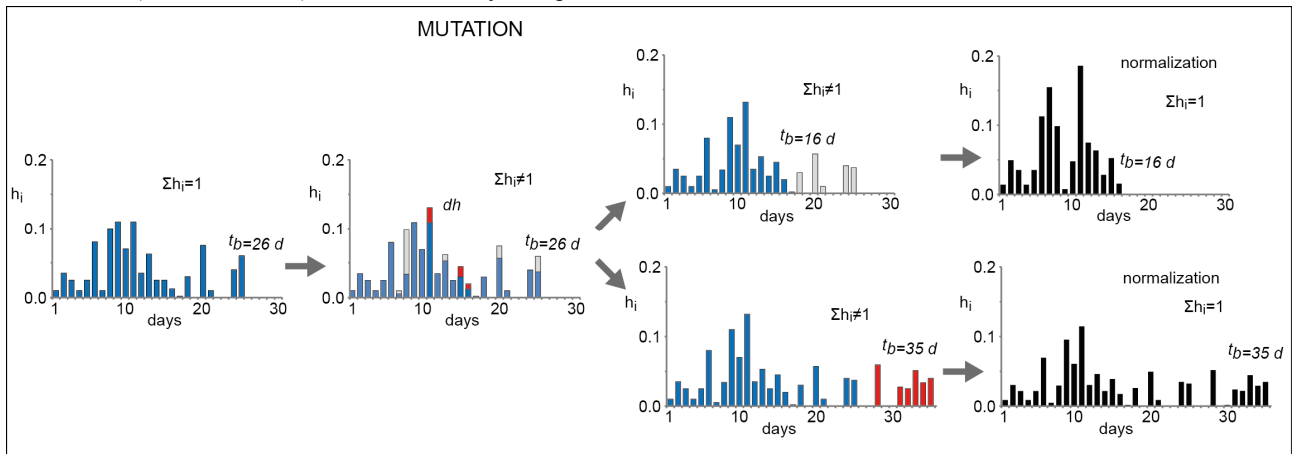
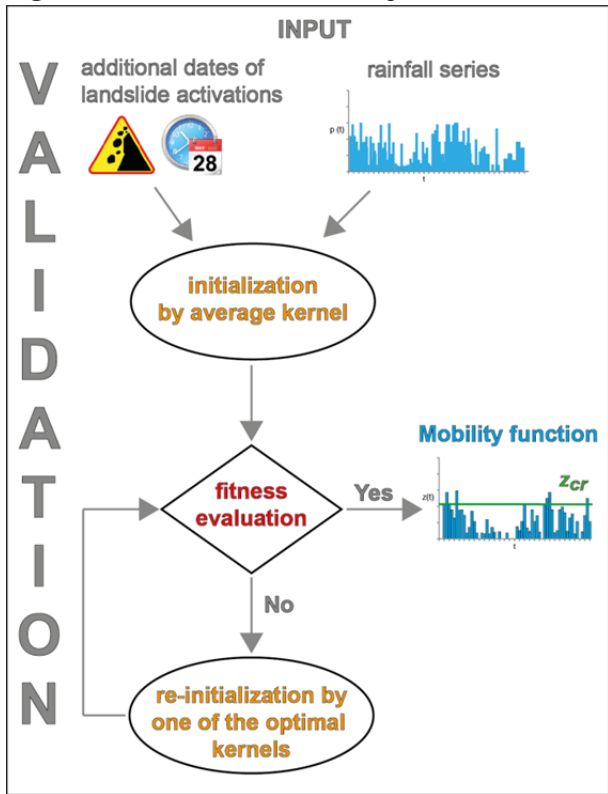
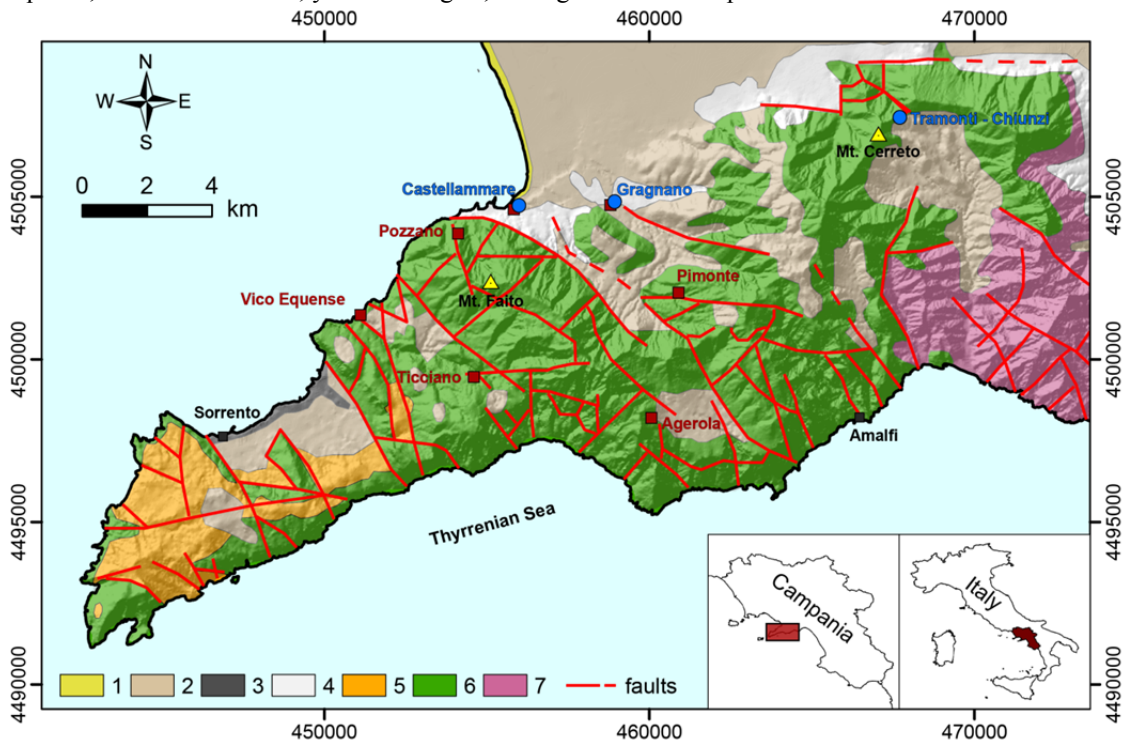


Figure 5. Scheme of the validation procedure of the model  $GA_{SAKe}$ .



**Figure 6.** Geological map of the Sorrento Peninsula (after Di Crescenzo and Santo, 1999, mod.). Key: 1) beach deposit (Holocene); 2) pyroclastic fall deposit (Late Pleistocene-Holocene); 3) Campanian ignimbrite (Late Pleistocene); 4) detrital alluvial deposit (Pleistocene); 5) flysch deposit (Miocene); 6) limestone (Mesozoic); 7) dolomitic limestone (Mesozoic). Red squares mark sites affected by shallow landslide activations; blue circles, the rain gauges; black squares, the main localities; yellow triangles, the highest mountain peaks.



**Figure 7.** Cumulative daily rainfall (in mm) during the 14 days preceding landslide occurrences. Key: in blu, red, and green = values from the Tramonti, Castellammare, and Tramonti-Chiunzi rain gauges, respectively. Numbers refer to id. in Table 1 (cf. first column).

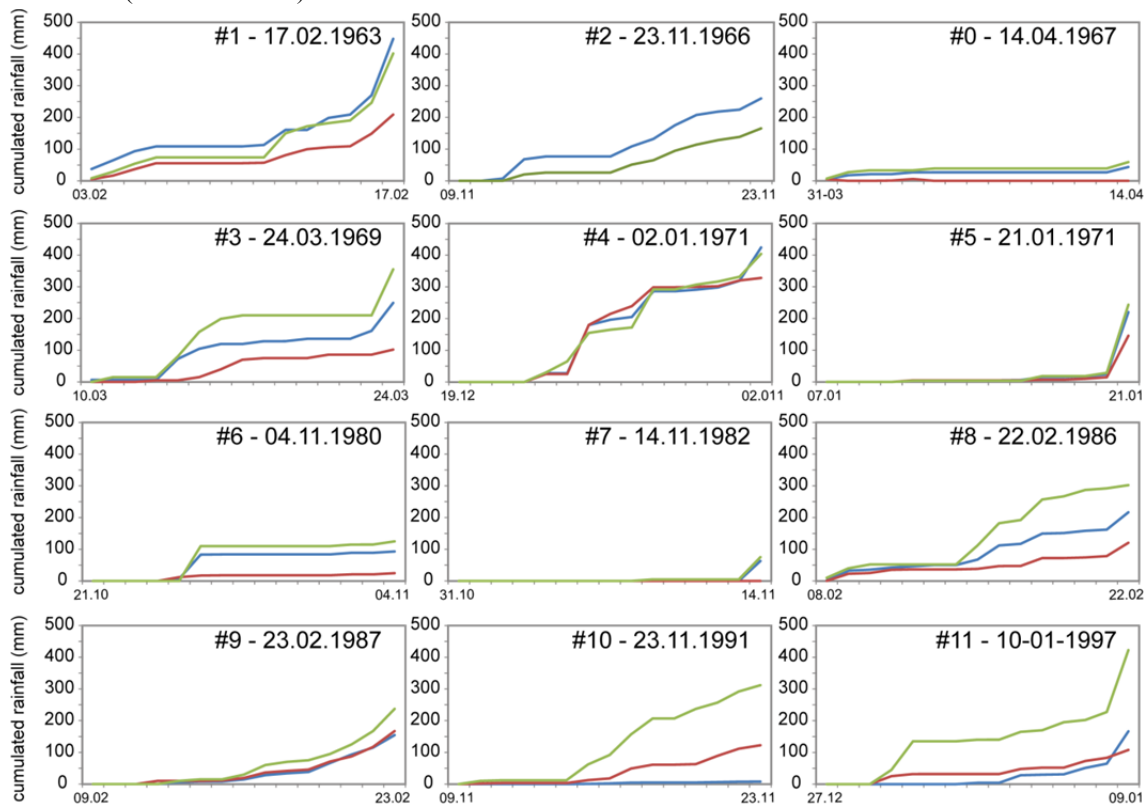


**Figure 8.** Location of the study area (red square: San Fili village; blue circle: Montalto Uffugo rain gauge). On bottom left, an extract from the geological map of Calabria (CASMEZ, 1967). Key: sbg gneiss and biotitic schist with garnet (Palaeozoic); sbm schist including abundant granite and pegmatite veins, forming migmatite zones (Palaeozoic);  $M_3^{ar}$  arenite and silt with calcarenite (Late Miocene);  $M_3^a$  marly clay with arenite and marls (Late Miocene);  $m_3^{cl}$  reddish conglomerate with arenite (Late Miocene);  $q^{cl}$  loose conglomerate of ancient fluvial terraces (Pleistocene). The site affected by the Uncino landslide is marked by a red star.

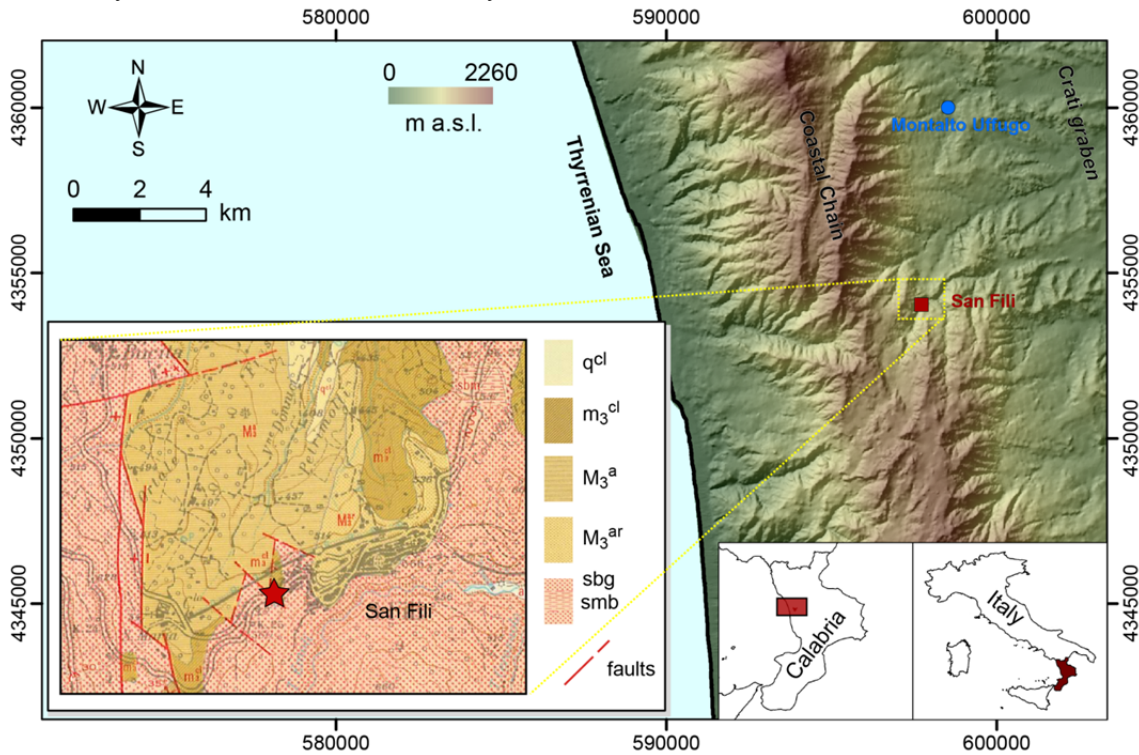


**Figure 9.** Cumulative daily rainfall (in mm) from 30 to 180 days before landslide occurrences (Montalto Uffugo gauge). Numbers refer to identification number (#) in Table 3 (cf. first column).

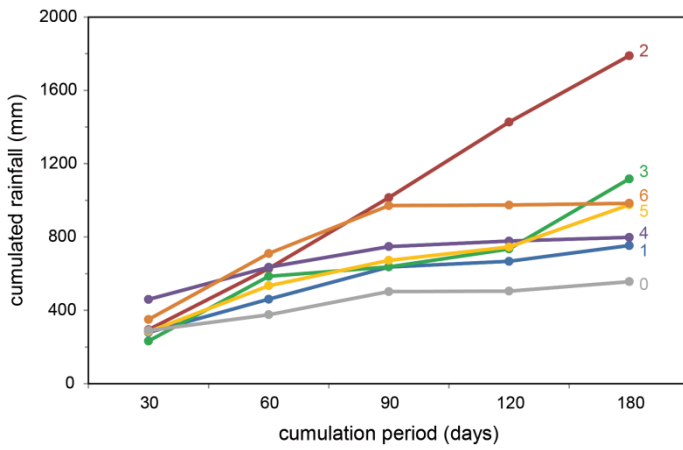


**Figure 10.** Sorrento Peninsula case study. Average kernel obtained from the best 100 filter functions.

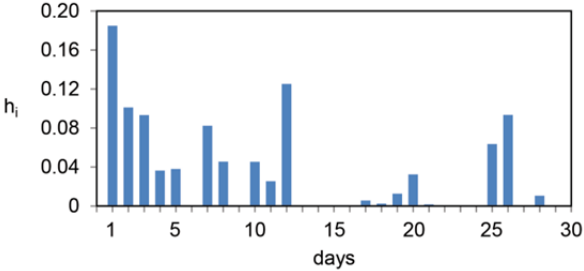




**Figure 11.** Sorrento Peninsula case study. Mobility function,  $z(t)$ , of the average kernel. The red line ( $z_{cr} = 22.53$ ) shows the maximum value of the mobility function (critical condition) that is unrelated to known landslide activations. The green line ( $z_{j-min} = 22.63$ ) – almost overlapping with the red line in this case – shows the minimum value of the mobility function related to known landslide activations. When the mobility function exceeds the threshold marked by the red line, landslide activation may occur. The red dots represent the maxima of the mobility function corresponding to the dates of landslide activation considered for calibration.

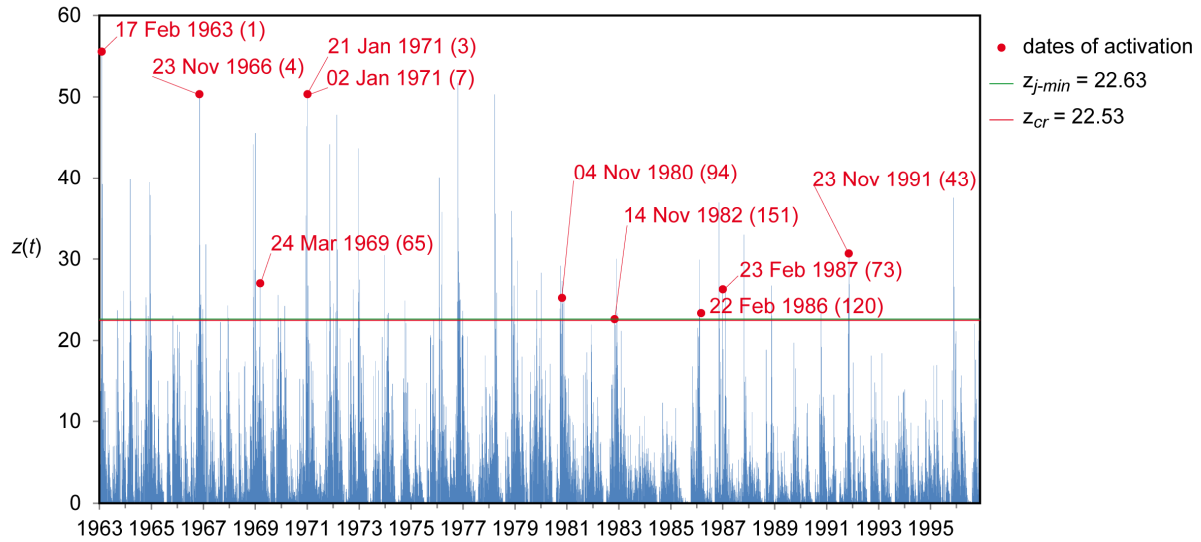


**Figure 12.** Sorrento Peninsula case study. Kernels providing (a) the best fitness ( $\Phi_{max} = 0.807$ ), (b) the minimum base time  $t_b \min$  (26 days), (c) the  $\Delta z_{cr} \max$  (0.00801), and (d) the minimum first order momentum,  $\mu_0 \min$  (9.460).

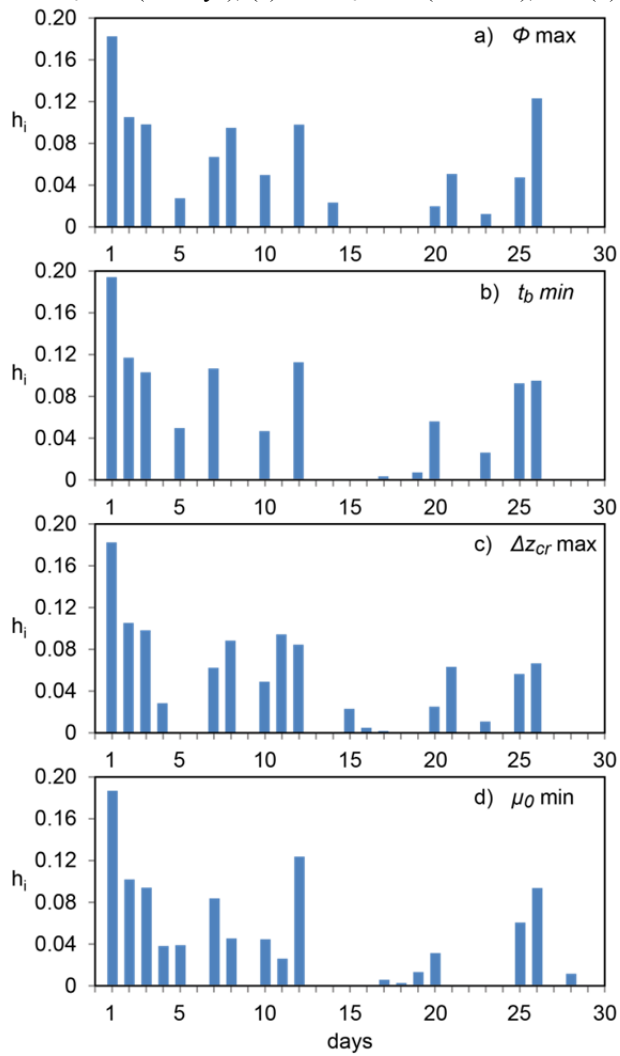


**Figure 13.** Sorrento Peninsula case study. a) Validation of the average kernel against the #11 event. b) Particular of Fig.13a, limited to the period  $\pm t_b$ , including the date of validation. Key as in Fig.11. The blue label indicates the date of validation. Grey background marks the period after the event that may be employed for re-calibration.

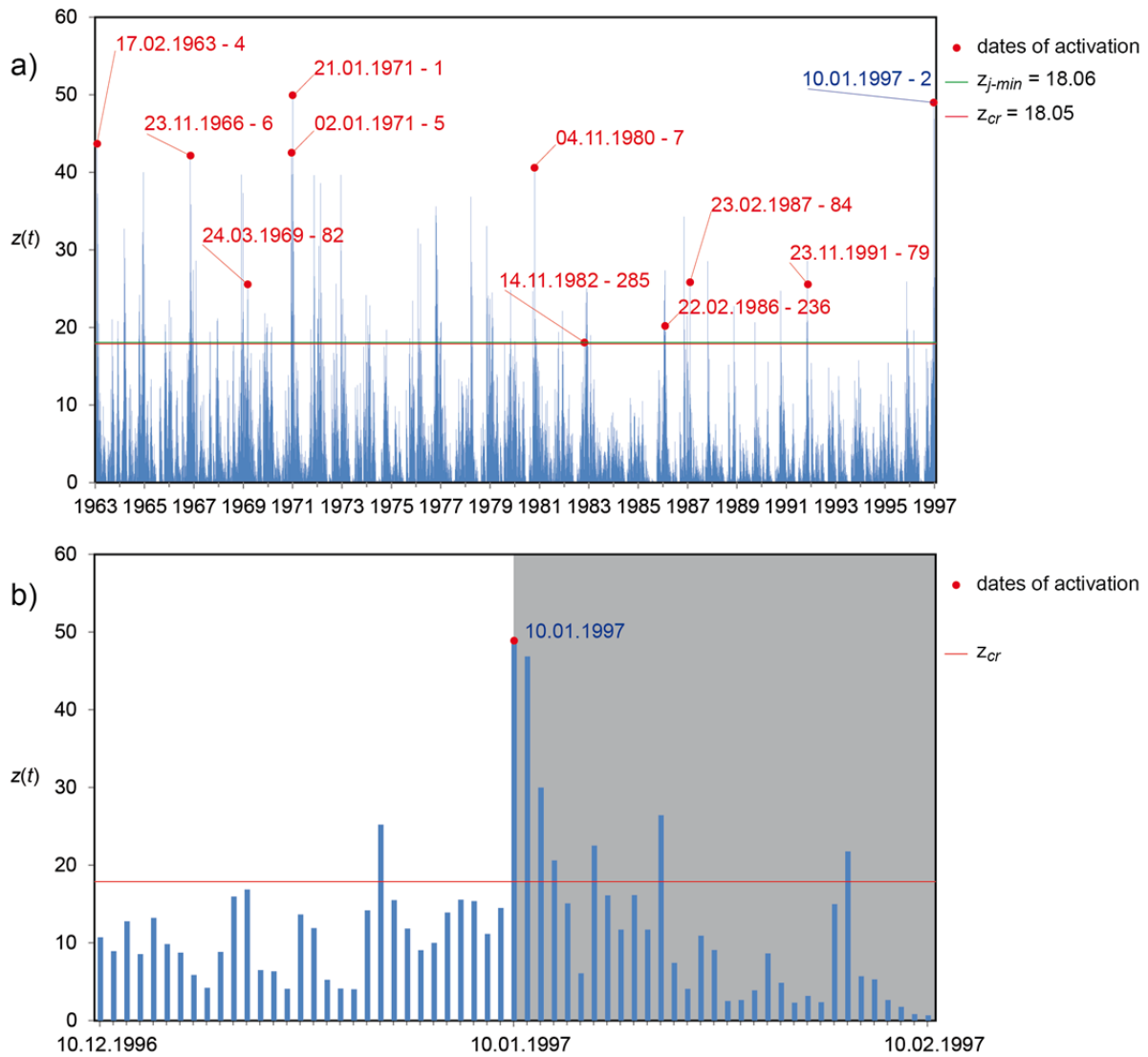


**Figure 14.** Uncino landslide case study. Average kernel obtained from the best 100 filter functions.

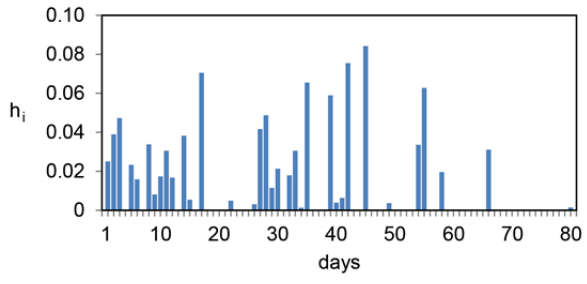


**Figure 15.** Uncino landslide case study. Mobility function,  $z(t)$ , of the average kernel. The red line ( $z_{cr} = 17.85$ ) shows the maximum value of the mobility function (critical condition) that is unrelated to known activations. The green line ( $z_{j-min} = 18.98$ ) shows the minimum value of the mobility function related to known activations. When the mobility function exceeds the threshold marked by the red line, landslide activation may occur. The red dots represent the maxima of the mobility function corresponding to dates of landslide activation considered for calibration.

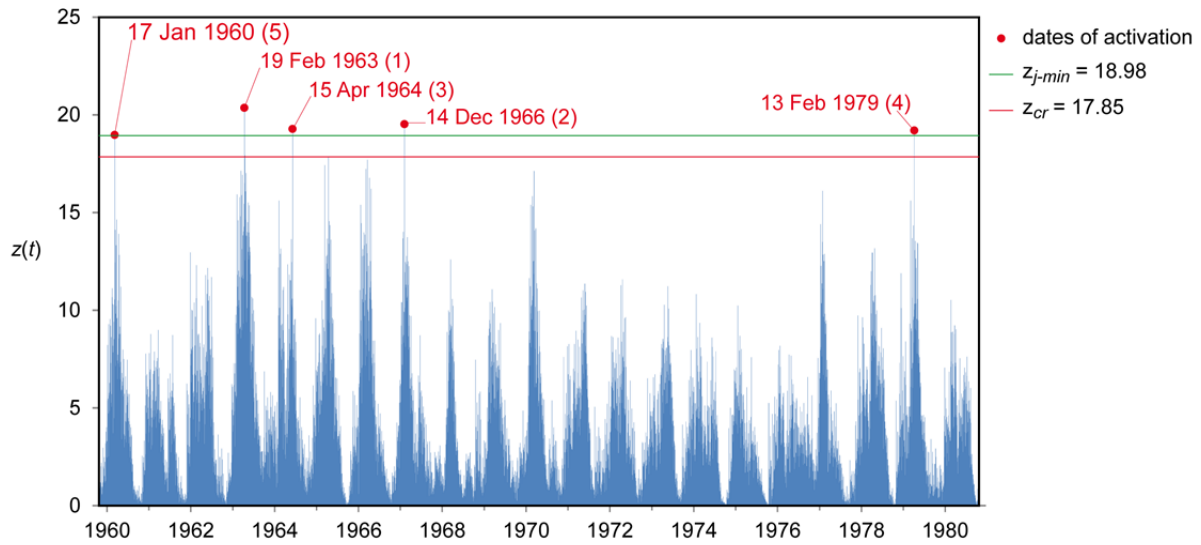


**Figure 16.** Uncino landslide case study. Kernel providing the best fitness.

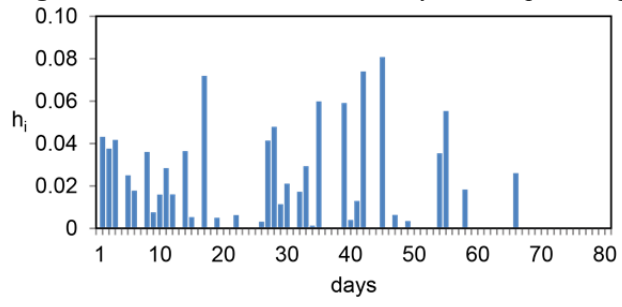


**Figure 17.** Uncino landslide case study. a) Validation of the average kernel against the #6 event. b) Particular of Fig.17a, limited to the period  $\pm t_b$  including the date of validation. Key as in Fig. 15. The blue label indicates the date of validation. Grey background marks the period after the event that may be employed for re-calibration.

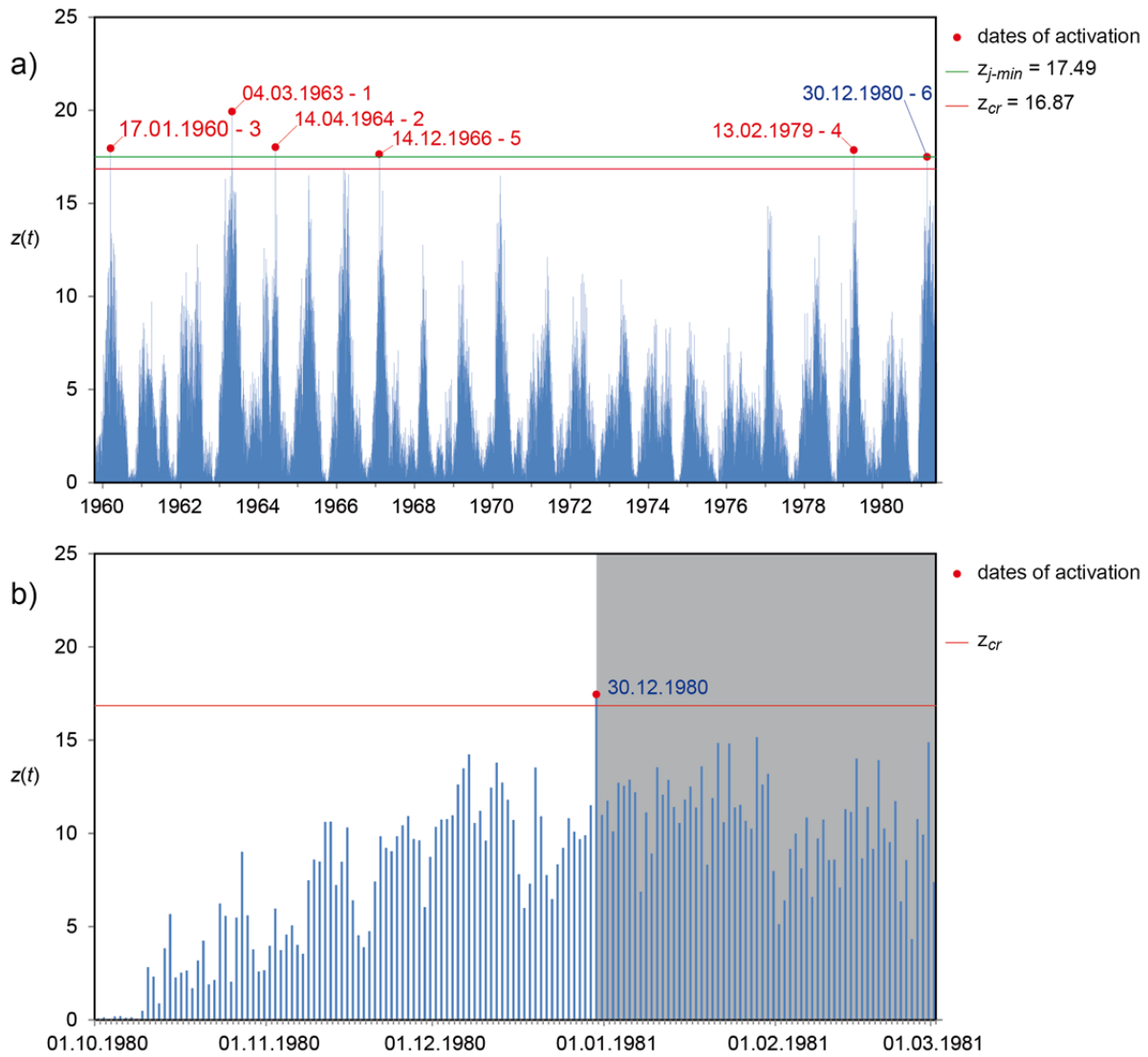


**Figure 18.** Uncino landslide case study. Average kernels obtained in calibration against the 2, 3, 4, 5, and 6 dates of activation.

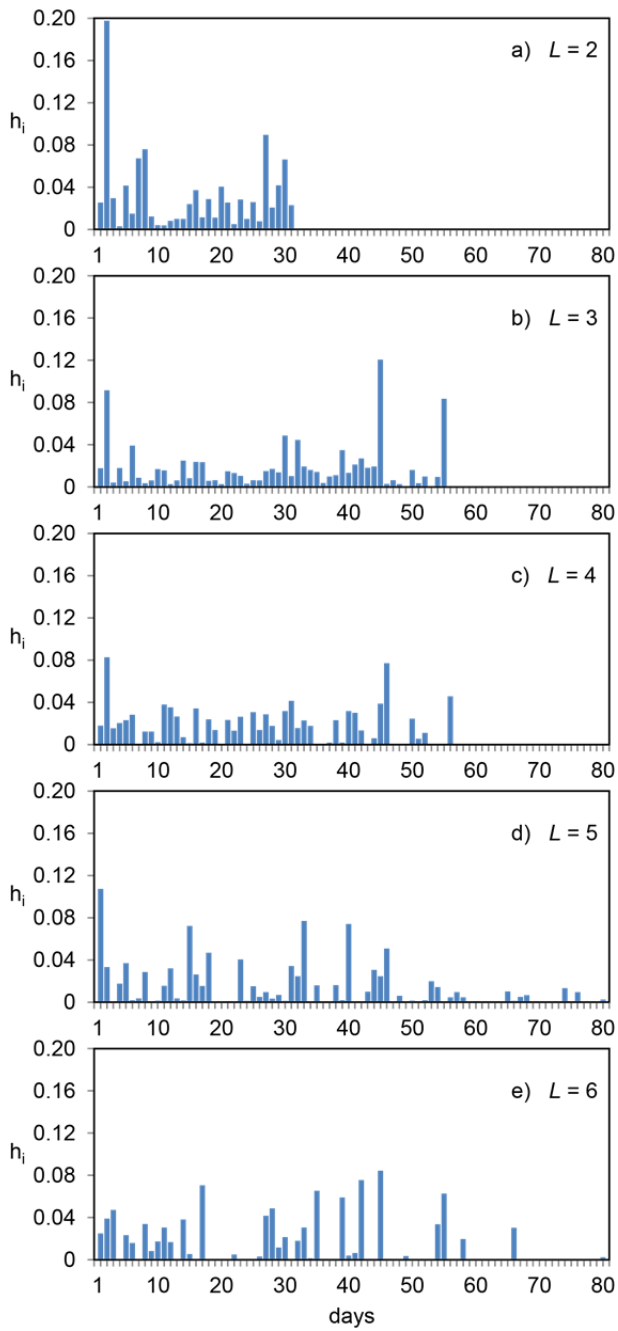




**Figure 19.** Maximum fitness ( $\Phi_{max}$ ), safety margin ( $\Delta z_{cr}$ ), number ( $n_i$ ) of iterations needed to first reach  $\Phi_{max}$ , and base time ( $t_b$ ) of the average kernel, based on GA parameters listed in Table 8.

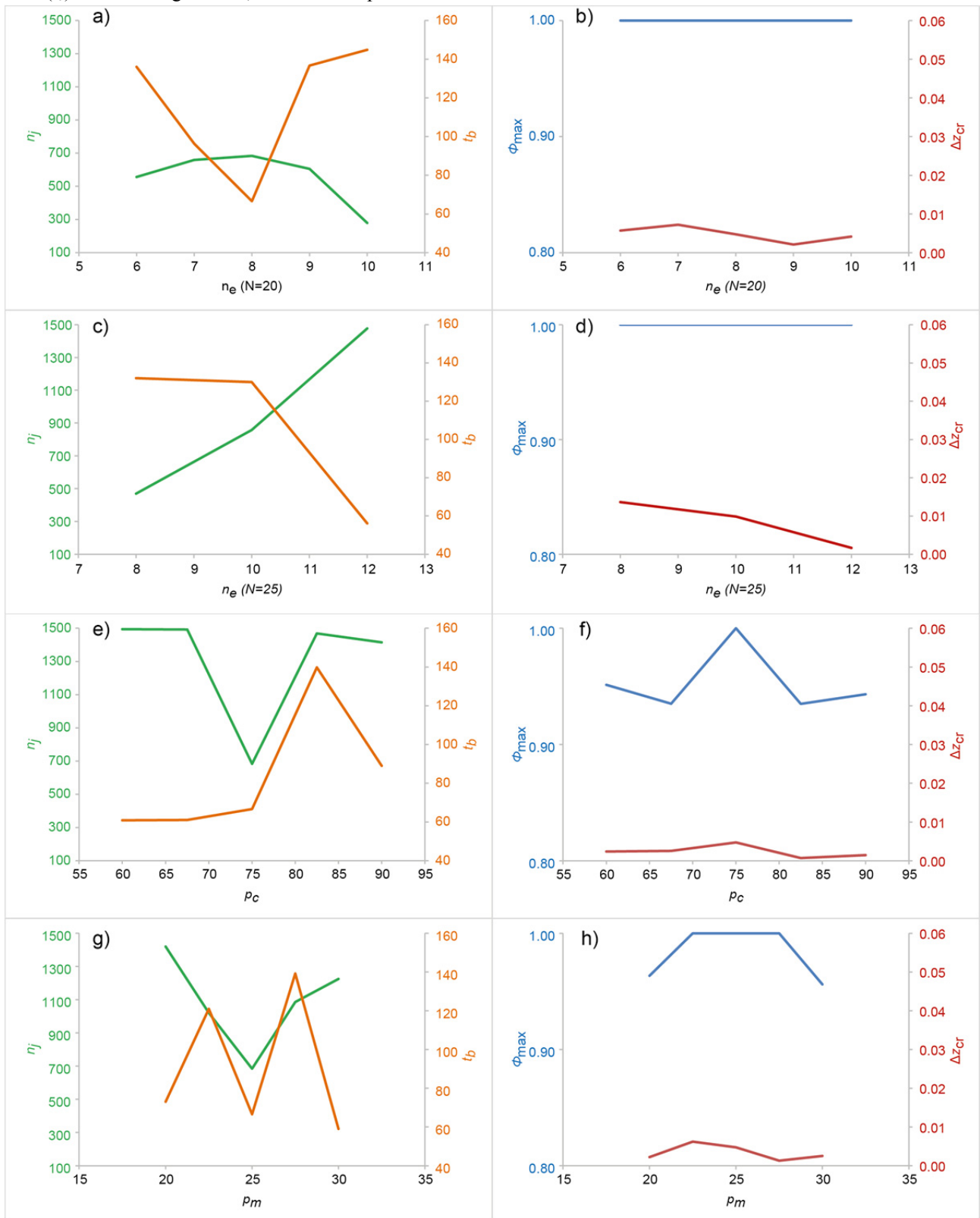


**Figure 19**

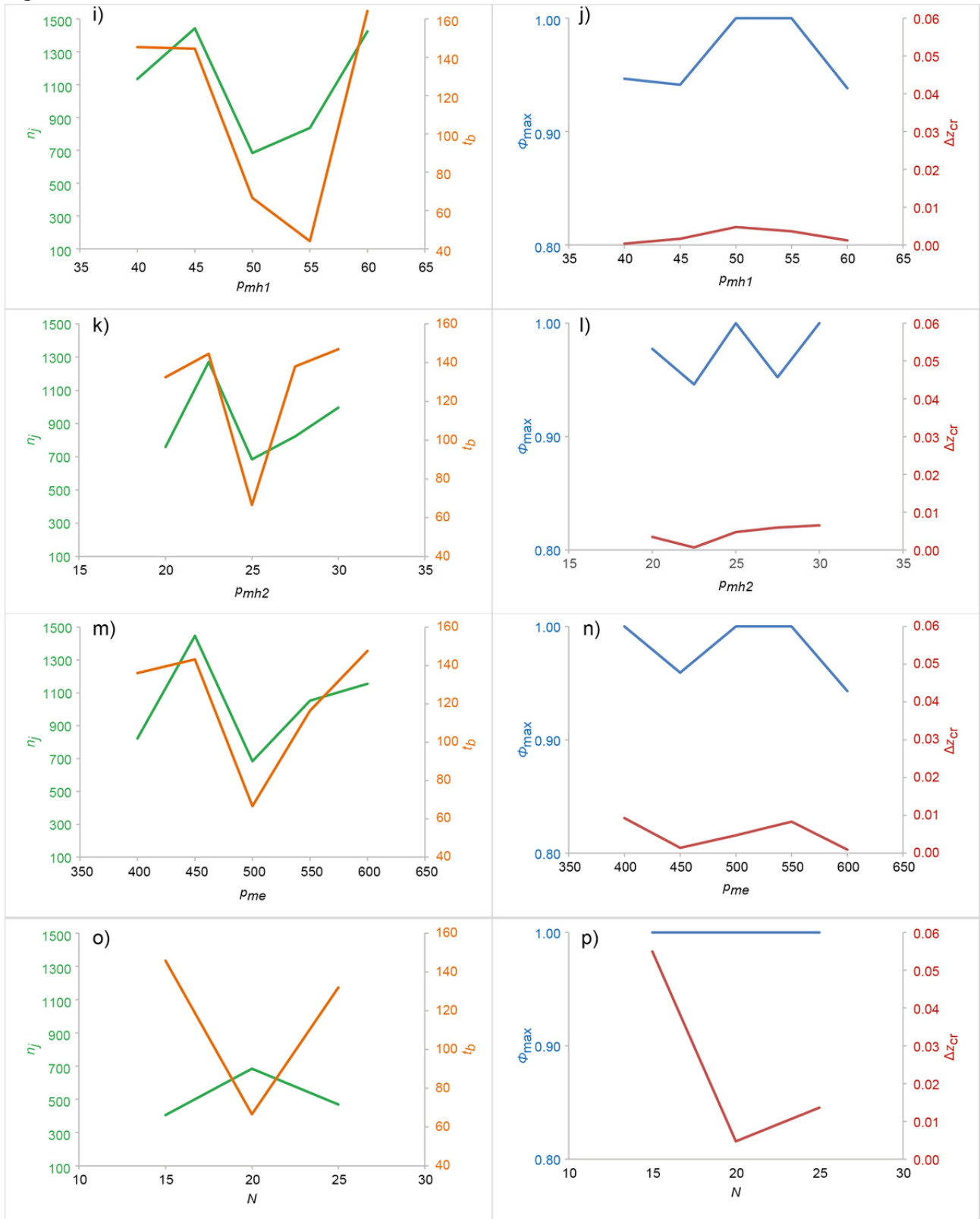


**Figure 20.** Uncino landslide case study. Results of progressive calibration. Variation of  $\Delta z_{cr}$  and  $\Phi_v$  for  $L$  increasing from 2 to 6.

